Geochemistry and petrogenesis of the mafic dyke swarm of the north eastern part of the Mesoproterozoic Irumide Fold Belt, North eastern Zambia

[1]Sakwiba Musiwa, [2]Frederick Akalemwa Kamona and [1]** Osbert N. Sikazwe

[1]Department of Geology, School of Mines, University of Zambia, Great East Road Campus, P.O. Box 32379, Lusaka, Zambia.

[2] Geology Department, University of Namibia.

*Corresponding author, **[1] Deceased

Tel: +260 978 368292   Email: sakwiba.musiwa@unza.zm

Abstract

The north eastern area of Zambia, that lies between Chama and Lundazi towns, is underlain by biotite gneisses of the Mesoproterozoic Irumide Fold Belt. The biotite gneisses are part of the Kampemba Group of the Irumide Fold Belt. A complex of mafic dyke swarm that appears to occupy a North East trending fracture zone occurs mainly between the two towns. The dykes have the same trend with the fracture zone. Individual dykes vary in size from about hundreds of metres long by a few 10s of metres wide, to about 4 kilometre long and about hundred metres wide. This study examined the petrogenesis of the mafic dyke swarm through the application of petrography, whole rock geochemistry as well as isotope geochemistry.

Fifteen fresh dyke swarm samples were sent to Actlabs in Canada for whole rock geochemical analysis. Three of the samples were analysed for Rb-Sr and Sm-Nd isotope geochemistry, and age determinations by K-Ar age dating method. The results received on age determination (geochronology) gave the ages, 1522 ± 90 Ma, 1067 ± 55 Ma and 608 ± 35 Ma. Sm and Nd grades ranged from $1.99 – 3.112$ ppm and $6.666 – 9.88$ ppm respectively. $_e$Nd were calculated by the laboratory at -5.23, -8.23 and -9.73. $^{87}Sr/^{86}Sr$ returned values of 0.710886, 0.714503 and 0.719612.

From the petrographic study of the thin sections, the studied dyke rocks were classified as gabbroic. They were composed mainly of plagioclase, clinopyroxene, hornblende with subordinate olivine, quartz, sericite, epidote and opaque phases. The dyke rocks occurred mainly in coarse and medium grained varieties and only two of the twelve samples examined, were fine grained.

Diagrams which were generated from whole rock geochemical data and the relative depletion of Nb and Ta to the other incompatible elements revealed that the dyke swarm was emplaced in a back arc continental subduction environment. The geochemical data further revealed that fractional crystallisation affected the magma of both types of rocks identified in the study, tholeiitic and calc-alkalis. Since no two samples came from the same dyke, it was deduced that all the mafic dykes in the study area experienced various levels of fractional crystallisation of possibly olivine, clinopyroxenes, plagioclase feldspars and hornblende.

Keywords: Petrogenesis, subduction, magmatism, dykes

Introduction

Dykes are believed to be the main conduits for magmas from great depths to shallower levels in the crust (Costa *et al.*, 2007; Munteanu *et al.*, 2017). Analysis of dyke swarms may provide invaluable information on the geodynamics of a particular geological environment in which they occur and may be sensitive indicators of certain fundamental geological processes (Halls, 1982; Fahrig, *et al.*, 1986; Sial, *et al.*, 1987; Sheraton and Sun, 1997; Maurice *et al.*, 2009; Srivastava *et al.*, 2014). Two sets of mafic and ultramafic dykes are reported in three Geological Survey of Zambia reports to occur mainly between Chama and Lundazi towns, in northeastern Zambia (Page, 1973; Oconur, 1976; Levington 1987). In the regional context, the area of northeastern Zambia between Chama and Lundazi, is underlain by rocks belonging to the Irumide Fold Belt (Figure 1), a Mesoproterozoic orogenic belt whose geology is dominated by biotite gneisses, which often show incipient migmatisation, that belong to the Kampemba Group (Page, 1973; O'Connor, 1976; Lewington, 1987). Page (1973), made a more concise record of the dykes that are found in the area he mapped. He reported that an earlier set of basic dykes was intruded in the Kampemba Group just before the end of tectonic activity and that the dykes were mildly metamorphosed to metagabbro, and deformed into large open folds. According to Page (1973), the metagabbro dykes occur as narrow ridges and that in their centres alteration is indicated by the mantling of the original clinopyroxene successively by a thick rim of uralite and a thin rim of hornblende. The margins of the dykes are more strongly metamorphosed and the pyroxene is completely replaced by hornblende and quartz (Page, 1973). Page (1973), stated that the second set of dykes post-date the Karoo faulting and are undeformed and unmetamorphosed.
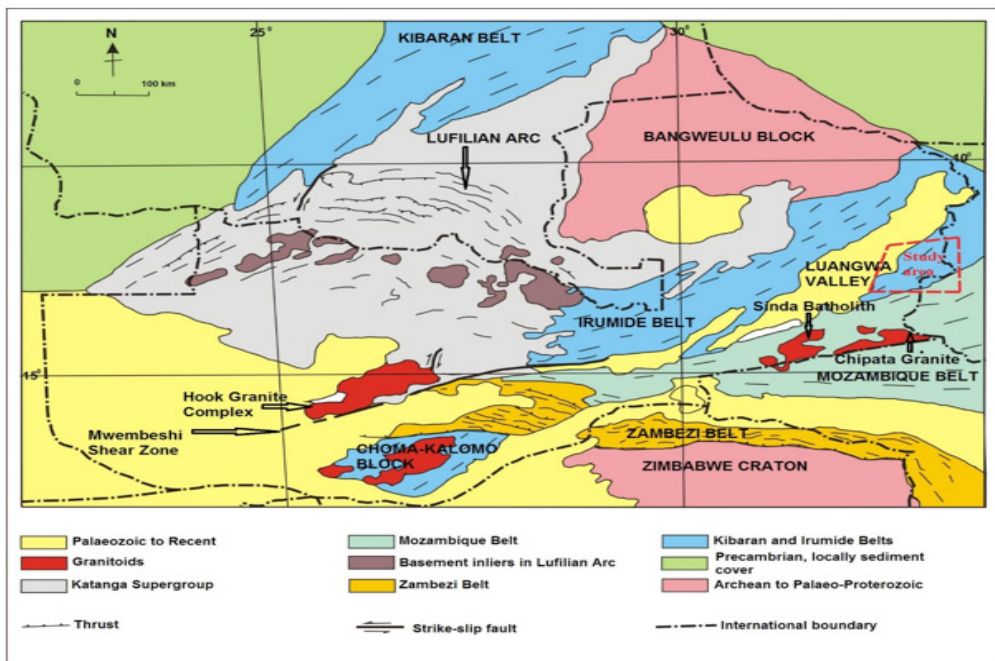

Figure 1: The geology and tectonic map of Zambia (modified after Porada, 1989).

Although the mafic dykes are well documented by previous researchers, they have not been studied in detail with regard to distribution, petrology, chemical composition, age and possible geodynamic evolution. Consequently, their contribution to the understanding of the geological evolution of the area where they occur is not well understood.

This article presents petrographic and whole rock geochemical (elemental and Sm-Nd; Rb-Sr isotopic) data, as well as geochronological data on the different pulses of dyke intrusions of the study area. Based on these data sets, the researchers present the chemical classification and interpretations of the petrogenesis of the mafic dykes. In presenting the petrogenesis, the researchers show possible crustal contamination, crystallisation fractionation, magma source and geotectonic environments of emplacement.

Methodology

Material or data source

In this study, freshly collected mafic dyke samples were used from which all the different types of data was extracted. Mafic rocks of the area are restricted to the dykes whose orientation is generally sub-parallel to the NE-SW structural fabric of the Irumide Fold Belt. They are generally exposed as large boulders with sharp edges (Figure 2), evidently with no sign of movement from the original positions of emplacement. They do not form any noticeable relief features, although in some places the dykes tend to form very low ridges which rise to only about one metre above the surrounding areas. Individual dykes range in size from a few hundreds of metres to about 4.5 kilometres in length, and a few tens of metres in width (Figure 3).
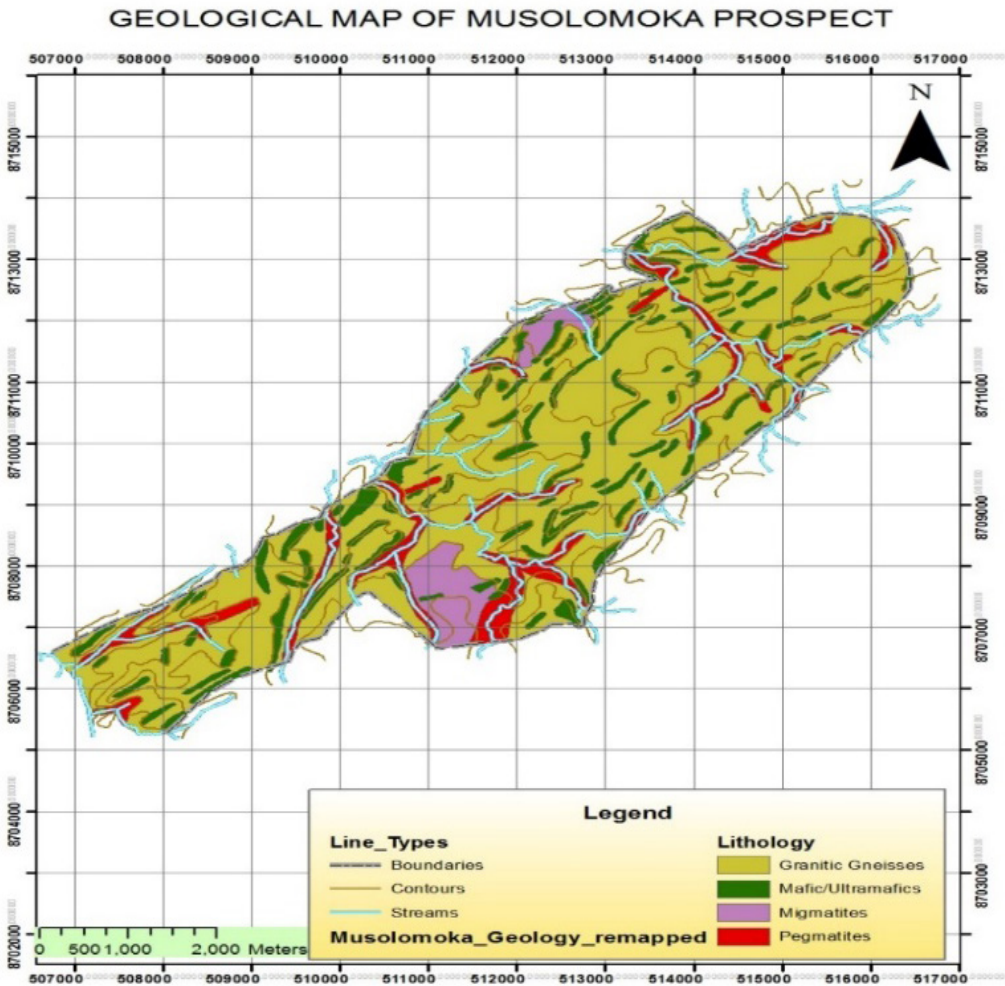

Figure 2: Typical mafic dyke outcrop.

Figure 3: Detailed geological map of Musolomoka Area showing a cluster of mafic dykes, between Chama and Lundazi (from Zawar Natural Resources 2015 exploration report).

Sampling method

A total of sixty two samples were collected over an area of about 75 km along the NE-SW strike, and about 4 km, wide (Figure 4). Fifteen of the collected samples were selected for geochemical and petrographic analysis.
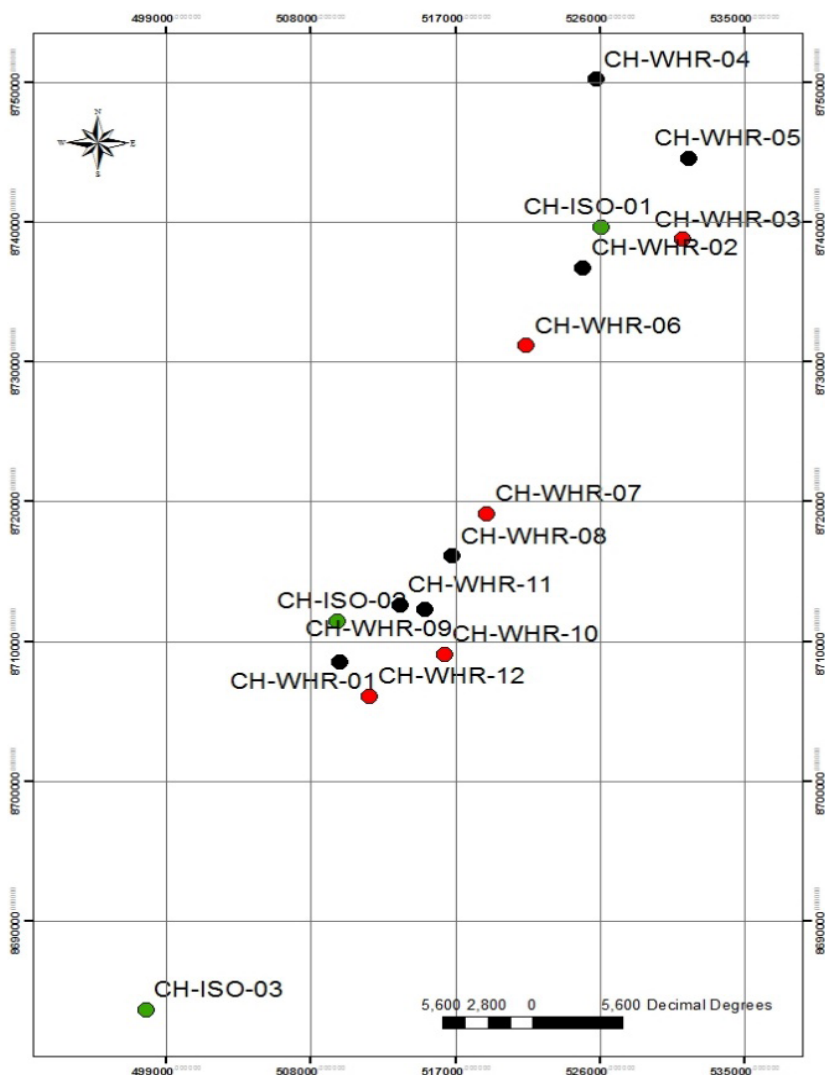
Figure 4: Sample locations for 15 samples which were sent for geochemical analysis; green = samples analysed for age dating and isotope geochemistry, red = samples which turned out to be of tholeiitic rocks, and black = samples which turned out to be of calc-alkalic rocks (UTM Projection, Zone 36L).

Petrography

Thin sections of the twelve samples, whose other portions were sent for whole rock geochemical analysis, were examined using petrographic microscopes.

Whole rock geochemistry

Twelve mafic dyke samples used in this study were analysed at the Activation Laboratories Limited, Ancaster, Ontario, Canada. Major elements and some trace elements including Sc, Be, V, Ba, Sr, Y, and Zr, were analysed by FUS-ICP. The rest of the trace elements and REE that include: Cr, Co, Ni, Cu, Zn, Ga, Ge, As, Rb, Nb, Mo, Ag, In, Sn, Sb, Cs,

La, Ce, Pr, Nd, Sm, Eu, Gd, Tb, Dy, Ho, Er, Tm, Yb, Lu, Hf, Ta, W, Tl, Pb, Bi, Th, and U were analysed by Fusion-Inductively Coupled Plasma-Mass Spectrometry (FUS-MS). On the geochemical results presented in table 1, total iron is shown as $Fe_2O_3^{(T)}$. The calculation of $Fe_2O_3^{(EST)}$, $FeO^{(EST)}$ and Mg# were adapted from Gill, (2011) as follows:

1) $FeO^{(T)} = Fe_2O_3^{(T)} \times 0.8998$
2) $FeO^{(EST)} = 0.9 \times FeO^{(T)}$
3) $Mg\# = 100 \times [MgO/(MgO+FeO^{(T)})]$

Methods of geochemical analysis and classification of rocks

Both major oxide and trace element variation of the sampled dykes were assessed by plotting index elements in each category; MgO and SiO_2, for the oxides, and Zr, for the trace elements, against other selected elements. The correlation factor or linear relationship was calculated using the free online Pearson correlation coefficient factor computation (Ciborowski, 2013). Element variables with coefficient factor values of $R \geq 0.75$ reflected good correlation, elements with coefficient factor values of $0.75 > R \geq 0.5$, were considered as moderately correlated, and elements with coefficient factor values of $R < 0.5$, were considered as poorly correlated.

The rocks were geochemically classified through the application of models of, (i) total alkali-silica (TAS) model diagram of Cox *et al.* (1979), (ii) SiO_2 Vs Na_2O+K_2O model of Irvine and Baragar(1971), and (iii) SiO_2 vs FeO/MgO classification plot of Miyashiro (1974). The geotectonic environment classification of the dykes was achieved by the application of Pearce *et al.* (1975)'s discrimination diagram of TiO_2-K_2O-P_2O_5. The geotectonic environments were further evaluated by the application of some trace and rare earth elements that included; Th, Hf, Ta, Yb, Y, Nb, La and Zr due to their particular usefulness in the studies of arc magmatism.

Petrogenetic processes, which included crustal contamination, fractional crystallisation and partial melting, were assessed through the application of various combinations of element variations and ratios. These were aided by plotting such combinations on known discrimination and variation models.

Isotope geochemistry and age dating

Rb-Sr methodology

The Rb and Sr concentrations as well as the $^{87}Sr/^{86}Sr$ and $^{87}Rb/^{86}Sr$ isotopic ratios were determined in the studied rocks using an isotope dilution technique with a mixed ^{85}Rb-^{84}Sr spike, which were added to the samples immediately before their chemical decomposition. Samples were dissolved in the $HF+HNO_3$ mixture under atmospheric pressure and a temperature of 80°C. Rb and Sr were separated using common chromatographic techniques. Extraction of the elements was carried out in 2.4 M HCl using the ion-exchange column filled with 3 mL of BioRad W50x8 (200–400 mesh) resin. Isotope ratios were measured on a Micromass Sector 54 multicollector TIMS (Thermo Scientific). The precision of results was controlled by the systematic analysis of SRM-987 international standard. The international standard (average measured value was $^{87}Sr/^{86}Sr$=0.710249±9 (2SD, n=5) during the period of the analysis). The $^{87}Sr/^{86}Sr$

and $^{87}Rb/^{86}Sr$ isotope ratios in the studied samples were measured with accuracy better than 0.002 and 0.5 rel. %, correspondingly.

Sm-Nd methodology

Nd isotope ratios were measured on a multi-collector Triton Plus TIMS (Thermo Fisher **Scientific). $^{147}Sm/^{144}Nd$ ratios were determined additionally by isotope-dilution method using $^{149}Sm-^{150}Nd$ mixed spike. About 100 mg of rock powder was dissolved in HF-HNO_3 mixture in microwave oven with addition of $^{149}Sm-^{150}Nd$ spike prior to dissolution for precise determination of $^{147}Sm/^{144}Nd$ in the samples. For Nd isotopic analysis, the REE were initially separated from major elements and Ba by cation exchange using Re resin (Eichrom Industries, Illinois, USA), before isolation of Nd and Sm following to. Ln resin (Eichrom Industries, Illinois, USA) was used for Nd and Sm isolation following to. Nd isotope ratios were measured in multidynamic collection mode. Isotope ratios were normalized to $^{146}Nd/^{144}Nd=0.7219$. Measured values in the international standard sample JNdi-1 ($^{143}Nd/^{144}Nd=0.512115$) were $^{143}Nd/^{144}Nd=0.512094\pm10$ (2SD, n=4) during the measurement period.

K-Ar methodology

Aliquots of the samples were weighted into Al container, loaded into sample system of extraction unit, degassed at ~100°C during 2 days to remove the surface gases. Argon was extracted from the sample in a double vacuum furnace at 1700°C. The determination of radiogenic argon content was carried out twice on MI-1201 IG mass-spectrometer by isotope dilution method with 38Ar as spike, which is introduced to the sample system prior to each extraction. The extracted gases were cleaned up in a twostep purification system. Then pure Ar is introduced into custom built magnetic sector mass spectrometer (Reinolds type). It shall be noted that the test was done twice per sample to ensure the consistency of the result. Two globally accepted standards (P-207 Muscovite and 1/65 "Asia" rhyolite matrix) were measured for 38Ar spike calibration. For age calculations the international values of constants were used as a follow up: λK=0.581*10-10y-1, λβ-=4.962*10-10y-1, 40K=0.01167 (at.%).

Results

Petrography

Petrographically, three varieties of mafic dykes were identified; the fine grained (two samples), the medium grained (four samples), and the coarse grained (six samples). The fine grained variety was equigranular and granoblastic with intergranular textures (Figure 5). This type was mineralogically dominated by plagioclase, clinopyroxenes, orthopyroxenes and hornblende with minor quantities of olivine, epidote and opaque minerals. Plagioclase was the most dominant (45-50%) with relict grains mostly <0.5 mm and about 0.5 mm for coarsely recrystallised and equant. Clinopyroxenes and orthopyroxenes formed about 30 per cent of fine grained variety, whilst hornblende formed about 10 to 15 per cent , occurring in different colours, but primarily reddish-brown, brown and green. Olivine formed less than 2 per cent of the phases present, whilst opaque minerals represented about 5 per cent of the fine grained variety.

Often, the fine grained dykes samples showed large phenocrysts of olivine and hornblende in a matrix of more hornblende, sericite, quartz and some opaque phase. The matrix is made of polycrystalline aggregates of anhedral crystals of the minerals which have clear grain boundaries. The large crystals of olivine and hornblende occur as either single crystals or aggregates of several crystals, especially hornblende. These phenocrysts suggest that they formed during fractional crystallisation of a magma in a deeper chamber and were transported with the melt during periodic tapping of the chamber and finally incorporated in the dykes. The large olivine crystals are characteristically altered to clinopyroxenes at the rims, giving them ragged edges.
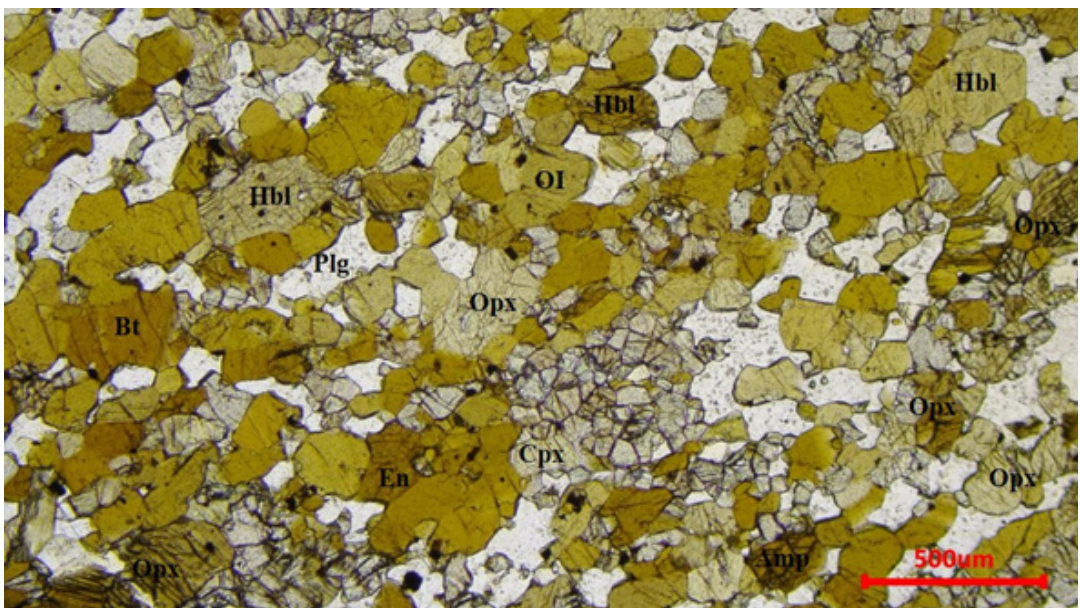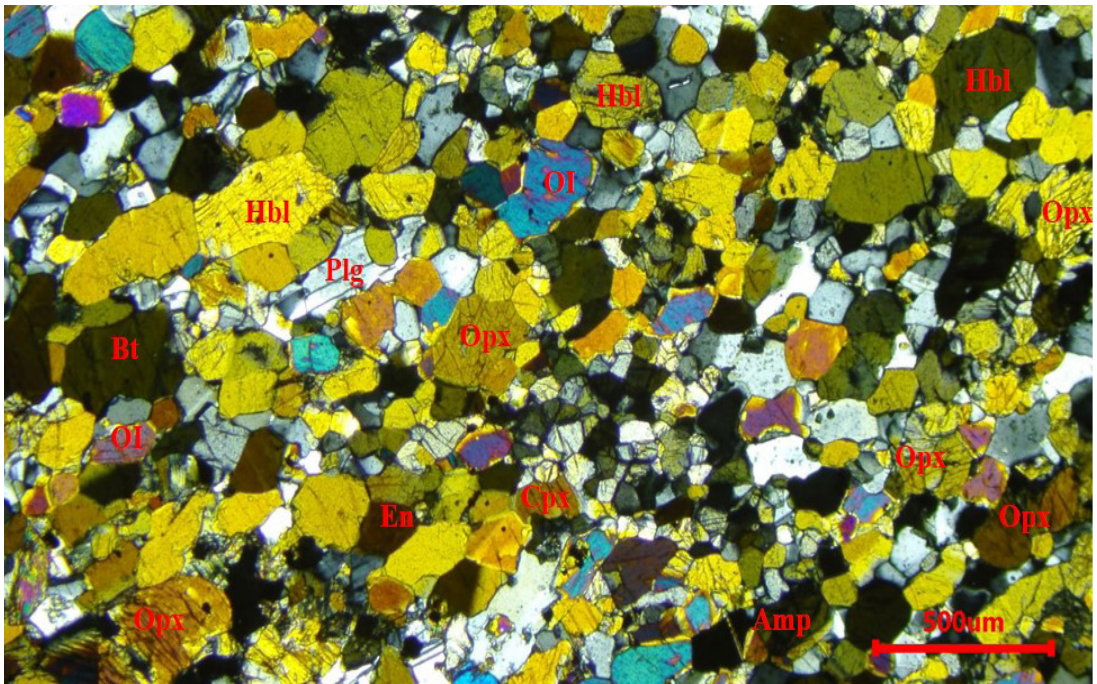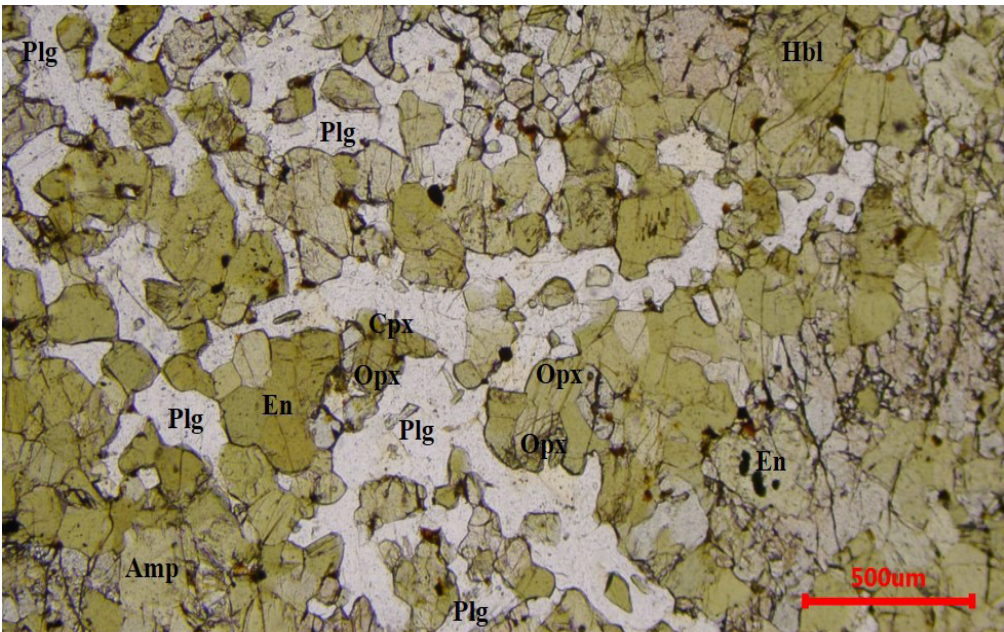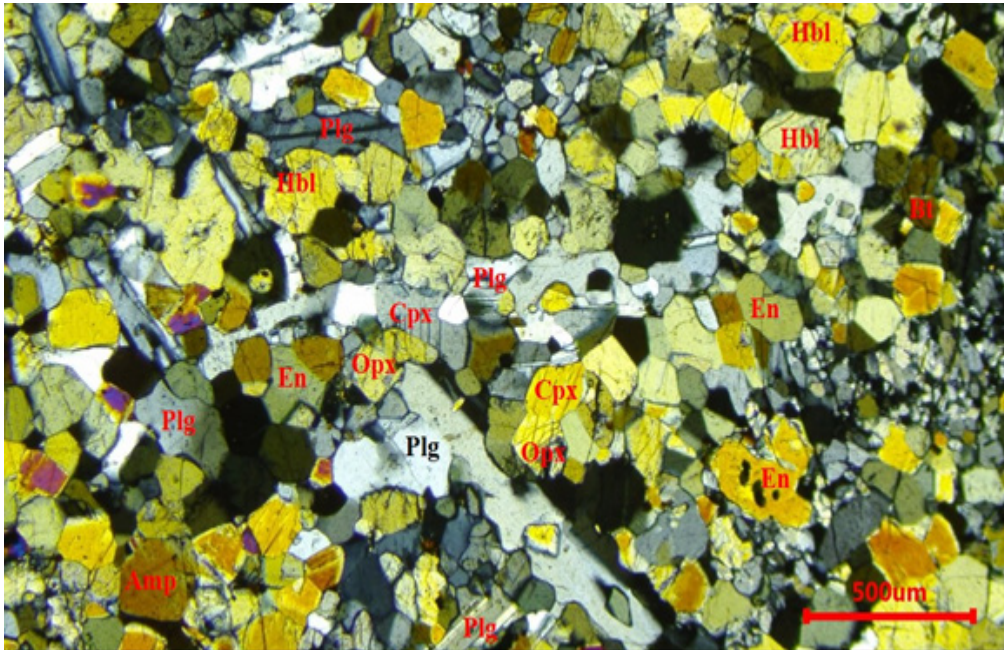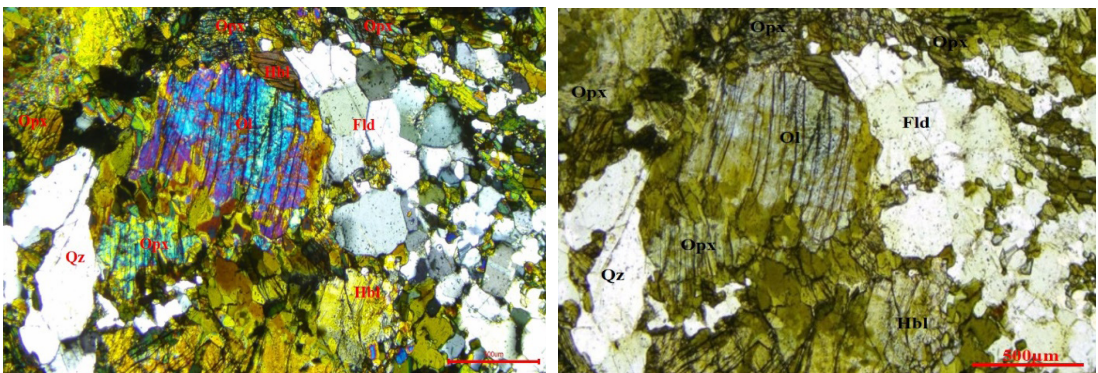
Figure 5: Photomcrographs (XPL and PPL) showing typical mineralogy and texture of the fine grained mafic dykes of the northeastern part of the Irumide Fold Belt, Northeastern Zambia. Cpx – clinopyeroxene, Opx – orthpyroxene, Hbl – horblende, Amp – amphibole (unclassified), Plg – plagioclase, Bt – biotite, Ol - olivine and En – enstatine. A. Granoblastic polygonal texture of the mafic dyke, with a weak foliation running diagonally from top right to bottom left of the picture. Plagioclase shows thick twin and grain boundaries, indicating grain boundary diffusion deformation. B. The intensity of deformation is similar to A, except temperature may have been higher. Grain boundary diffusion is dominant.

The medium grained variety was also dominated by plagioclase, clinopyroxenes, orhopyroxenes and hornblende with subordinate olivine, quartz, epidote and sericite (Figure 6). Plagioclase was noticeably less in that type than in the fine grained variety (about 40%). It predominantly occurred as lath-like micro-phenocrysts with ragged grain boundaries. Clinopyroxenes and orhopyroxenes ranged from about 15 to 30 per cent, where as hornblende ranged between about 5 to 10 per cent, occurring as brown blebs in clinopyroxenes and as cores to green hornblende either replacing a mafic mineral or rimming it. Olivine formed about 2 per cent, and epidote, 2 to 5 per cent, was markedly more in two of the four samples. Opaques and probably apatite (about 3-5%) were concentrated together in zones occurring in anhedral grains as veins or fillers parallel to foliation.

Similar to the fine grained variety, some of the medium grained dykes samples showed large phenocrysts of olivine and hornblende in a matrix of more hornblende, sericite, quartz and some opaque phase. The matrix had a similar texture found in the fine grained variety of aggregates of anhedral crystals of the minerals which have clear grain boundaries. The features of large crystals of olivine and hornblende occurring as either single crystals or aggregates of several crystals, were also observed in this variety. Epidote was markedly more in the two of the four medium grained samples and exhibited subhedral to euhedral crystals, where it appears to have totally replaced hornblende (see Figures 6C and D). The crystal contacts of the two minerals were sharp, giving the impression that epidote was not replacing hornblende from the edges. Hornblende replacing olivine and augite indicated that some of the portions of the dykes could be classified as an alkaline olivine gabbro. It is well observed that the hornblende rims are brown on augite and green on parts of the olivine (see Figure 6D). The green hornblende may be low in titanium, contrasting with the brown high-titanium hornblende. Clinopyroxene is possibly inverted sub-calcic augite.
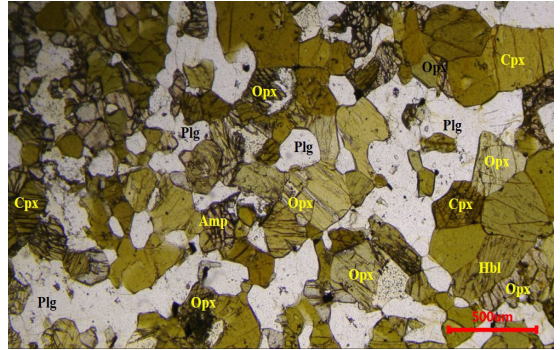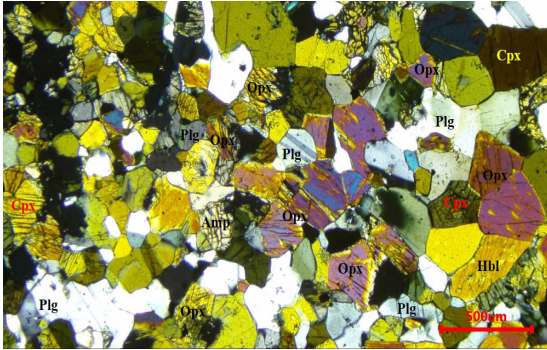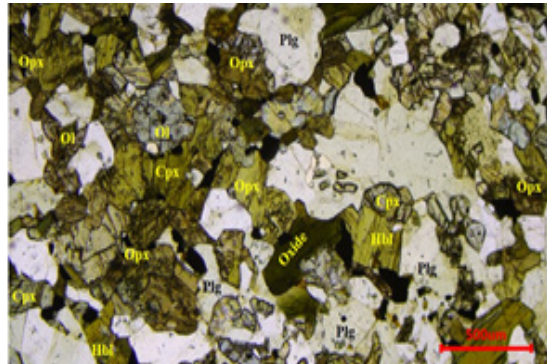
A
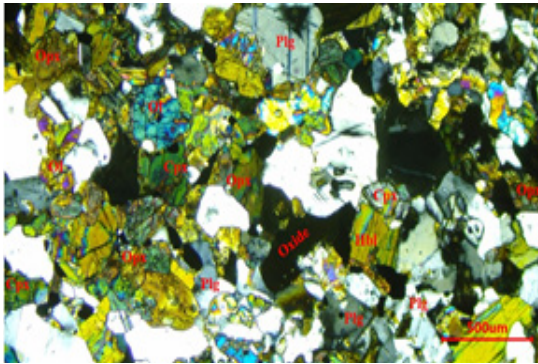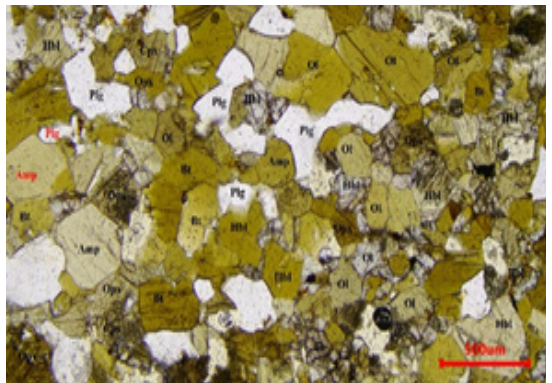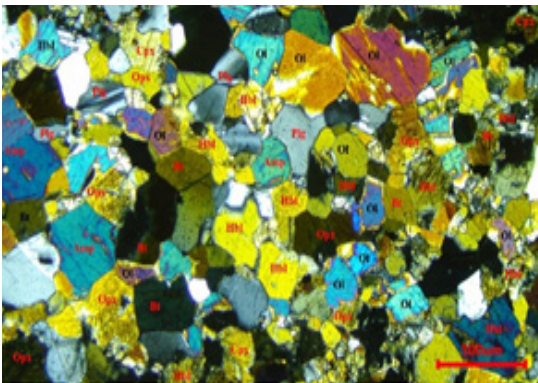
Figure 6: Photomicrographs (XPL and PPL) showing typical mineralogy and texture of the medium grained mafic dykes part northeastern part of the Irumide Fold Belt, Northeastern Zambia. Cpx – clinopyeroxene, Opx – orthpyroxene, Hbl – horblende, Amp – amphibole (unclassified), Ol – olivine, Bt – biotite, and Plg - plagioclase. The dyke rocks show a general granoblastic texture. Plagioclase is characteristic of thick rims, indicating diffusion and high temperature deformation, in all the dyke rock samples. The clear contacts between hornblende and epidote in C and D, indicate that epidote was not replacing hornblende from the edges.

In the coarse grained variety (six samples) the mineralogy was dominated by plagioclase, clinopyroxenes, orhopyroxene and hornblende, with subordinate sericite, opaques and epidote (Figure 7). Plagioclase (40 to 60%) was moderately to well-developed granoblastic in texture, with tapered polysynthetic twins in greater than 75 per cent of the grains. Clinopyroxenes (25 to 35%)occurred in grains which were predominantly 1mm or larger, poikilitic and may have been interstitial to plagioclase. Hornblende, about 20 per cent by volume, often occurred in aggregates measuring 4 mm or more, whilst olivine was less than 2 per cent. Opaque and other minor minerals comprised about 2 per cent of the coarse grained examined dyke samples. Probably very close to solidus temperatures, olivine and augite reacted with the hydrous residual liquid to grow hornblende rims on both of them (see Figure 7E). Imperfections in the augite, possibly trapped liquid inclusions or exsolution lamellae (see Figure 7E), also reacted to grow hornblende within augite crystals. It is well observed that the hornblende rims are brown on augite and green on parts of the olivine (see Figure 7D). The green hornblende may be low in titanium, contrasting with the brown high-titanium hornblende. Clinopyroxene is possibly inverted sub-calcic augite. Cleavage, exsolution lamellae and minor alteration along cracks are prominent features of the clinopyroxene. It is the coarsest-grained mineral in the rocks, but there is some recrystallisation (see Figure 7A). In some samples, plagioclase grains are subhedral, but olivine and clinopyroxene are anhedral. In Figure 7F, plagioclase grain shape is generally subhedral with sharp and straight to very curvilinear and muted boundaries with other plagioclase/microline grains. However, olivine is less than 3 per cent medium grained, subhedral granoblastic, in the same sample (see Figure 7F), and clinopyroxene is less than 10 per cent, medium grained, subhedral, some contain stringers at a very reddish-brown phase, oxide of some sort may be. Anhedral opaques may be included in clinopyroxene, whilst brown hornblende as anhedral grains, form in cracks of olivine, also as anhedral blebs in talc aggregates (see Figure 7F). What is present is the mesocumulate texture, in which liquid trapped between cumulate crystals was able to exchange material with the nearby magma, allowing more extensive overgrowths of cumulate minerals and a smaller volume of ultimately trapped liquid (see Figure 7E). Small grains of olivine, clinopyroxene, and apatite indicate the original trapped liquid. Probably very close to solidus temperatures, olivine and augite reacted with the hydrous residual liquid to grow hornblende rims on both of them (see Figure 7E). Imperfections in the augite, possibly trapped liquid inclusions or exsolution lamellae (see Figure 7E), also reacted to grow hornblende within augite crystals.
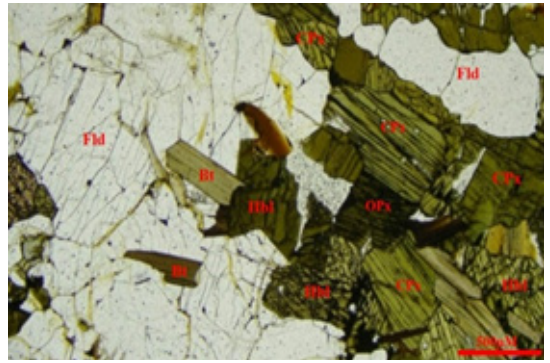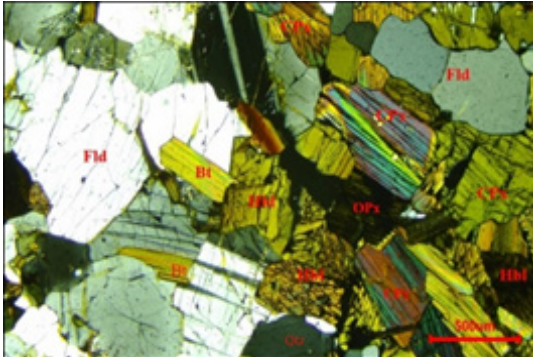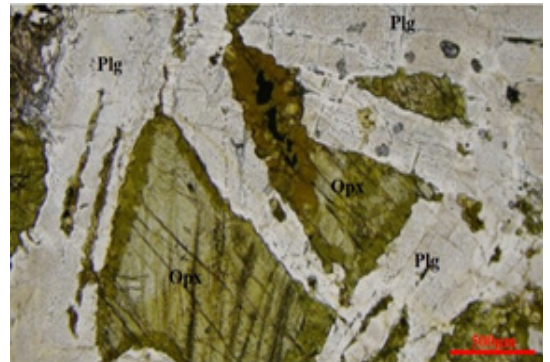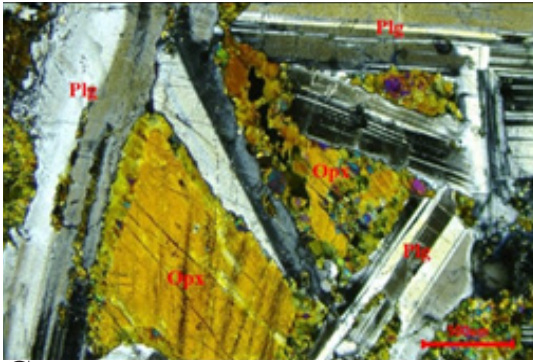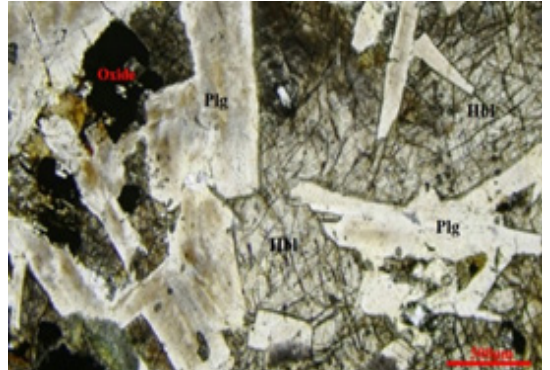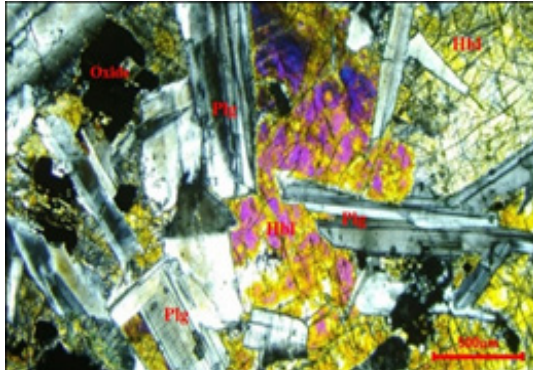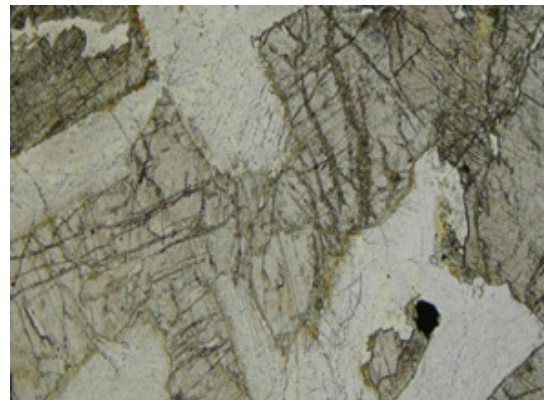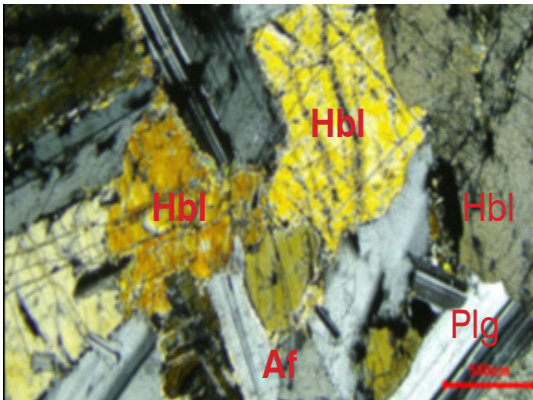
E
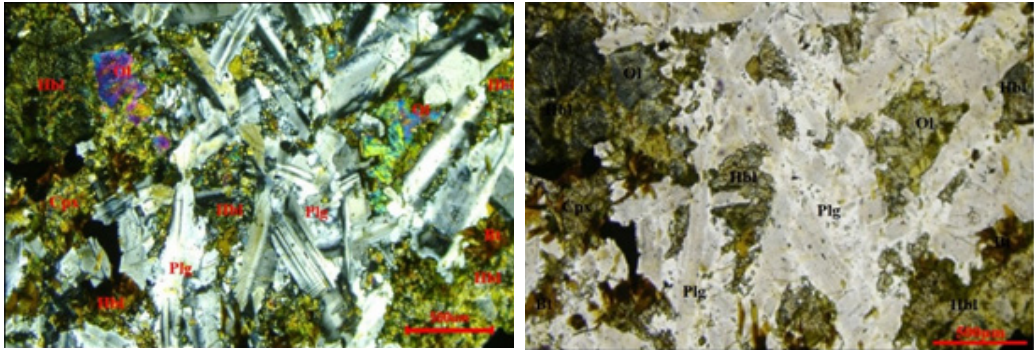
F
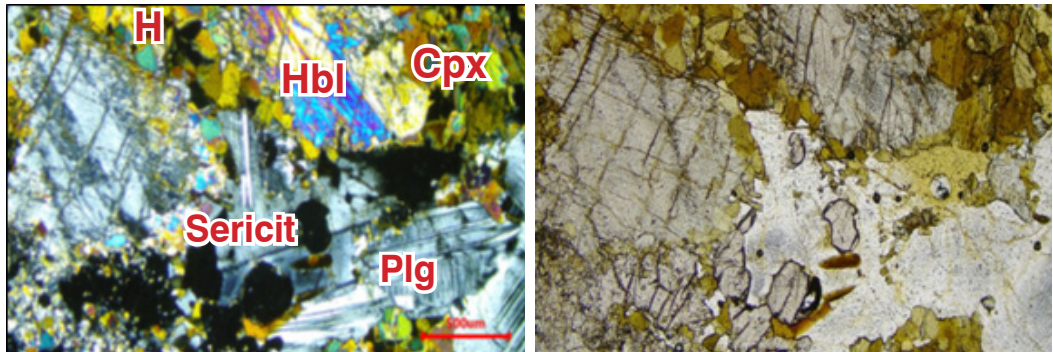
Figure 7: Photomicrographs (XPL and PPL) showing typical mineralogy and texture of the couarse grained mafic dykes of the northeastern part of the Irumide Fold Belt, Northeastern Zambia. Cpx – clinopyeroxene, Opx – orthpyroxene, Hbl – horblende, Bt – biotite, and Plg – plagioclase.

Whole rock Geochemistry

The whole-rock geochemical results of the samples that were collected and analysed from the study area, are shown in Table 1.The samples showed a narrow SiO_2 variation content range of 44.28 to 50.32 wt. per cent, whilst MgO content showed a wide variation ranging between 5.64 to 15.39 wt. per cent. Calculated Mg# also showed a wide variation with values ranging between 29.7 and 58.0. Total alkali content ranged between 1.57 and 3.78 wt. per cent. The Al_2O_3 content ranged between 13.48 to 17.47 wt. per cent.TiO_2 content also showed wide variation of values ranging between 0.766 to 2.903 wt. per cent. The other oxides exhibited the following ranges: Fe_2O_3(T), 13.48 to 17.47 wt. per cent; MnO, 0.148 to 0.2 wt. per cent; CaO, 8.81 to 11.37 wt. per cent; Na_2O, 1.33 to 2.74 wt. per cent; K_2O, 0.21 to 1.04 wt. per cent; and P_2O_5, 0.07 to 0.36 wtper cent. Loss on ignition (LOI) values ranged between -0.31 to 1.06 wt. per cent.

Three main compatible trace elements, Ni, Cr, and Co vary as follows: Ni, 80 to 720 ppm; Cr, 150 to 1400 ppm; and Co, 43 to 84 ppm. Selected incompatible trace elements also vary widely as : Zr, 43 to 174 ppm; Sr, 91 to 325 ppm; Rb, 6 to 41 ppm; Nb, 2 to 23 ppm; Y, 17 to 29 ppm; Hf, 1.3 to 4.4 ppm and Th, 0.8 to 4.4 ppm.

Table 1: Whole rock elemental chemistry of the samples of the Study area (major element oxides are in wt.%, trace elements are ppm)

Sample	WHR-01	WHR-02	WHR-03	WHR-04	WHR-05	WHR-06	WHR-07	WHR-08	WHR-09	WHR-10	WHR-11	WHR-12	ISO-01	ISO-02	ISO-03
SiO2	47	47.2	48.8	46.8	50.3	48.2	48	44.7	47.1	49.6	45.1	45.8			
Al$_2$O$_3$	14.5	16.9	15	16.3	17.1	17	14.4	14.5	17.5	16.3	13.5	13.7			
Fe$_2$O$_3$(T)	15.4	12.7	15.2	13.5	9.57	14.8	16	16	12.3	12.5	12.4	12.5			
MnO	0.2	0.17	0.19	0.18	0.15	0.19	0.19	0.19	0.17	0.18	0.18	0.18			
MgO	12.2	8.01	5.8	8.64	6.95	6.59	6.44	12	8.43	5.64	15.4	11.4			
CaO	10	11.3	8.81	10.7	11.3	10.8	10.9	9.3	10.1	9.61	9.2	10.8			
Na2O	1.85	2.49	2.74	2.18	1.97	2.4	2.52	1.79	2.53	2.58	1.33	2.18			
K2O	0.21	0.35	1.04	0.42	0.64	0.46	0.42	0.29	0.49	1.01	0.24	0.42			
TiO2	1.62	1.36	2.77	1.46	0.77	2.9	2.5	1.37	1	1.68	0.87	1.43			
P2O5	0.11	0.12	0.36	0.11	0.08	0.27	0.21	0.1	0.09	0.16	0.07	0.15			
LOI	0.1	0.07	-0.31	0.28	0.27	0.01	0.12	0.53	0.64	0.32	0.5	1.06			
Total	101	101	100	101	99.2	101	99.9	99	100	99.5	98.8	99.5			
Sc	34	35	28	34	34	34	34	35	39	31	30	34			
Be	1	1	2	1	1	1	1	1	1	1	1	1			
V	344	278	341	302	212	351	335	294	244	325	236	268	256	275	206
Cr	760	380	210	500	240	260	160	430	190	150	1140	530	1400	640	760
Co	84	58	55	61	45	53	48	72	59	43	80	63	73	77	75
Ni	520	170	230	210	150	120	100	440	290	80	720	280	520	410	530
Cu	130	130	110	140	110	180	170	130	130	100	110	90	560	150	170
Zn	100	90	140	100	70	130	100	90	80	90	70	90	90	90	80
Ga	19	20	23	20	18	22	20	19	18	23	16	18	15	17	15
Ge	2	2	2	2	2	2	1	2	2	2	1	2	1	1	2
As	4	4	4	4	4	4	4	4	4	4	4	4	4	4	4
Rb	6	11	35	14	25	12	11	9	16	41	9	9	12	14	16
Sr	198	217	325	218	154	317	312	202	171	300	135	259	97	144	91
Y	20	17	29	19	18	26	27	21	25	21	17	17	23	22	18
Zr	88	68	174	82	59	151	132	80	70	80	53	78	53	72	43
Nb	2	2	17	2	3	23	16	3	3	9	2	13	2	2	2
Mo	1	1	1	1	1	1	1.5	1.5	1.5	1.5	1.5	1.5	3	1	1
Ag	0.4	0.4	0.8	0.4	0.4	0.7	0.4	0.4	0.4	0.4	0.4	0.4	0.4	0.4	0.4
In	0.1	0.1	0.1	0.1	0.1	0.1	0.1	0.1	0.1	0.1	0.1	0.1	0.2	0.1	0.1
Sn	1	1	2	1	1	2	1	1	1	1	1	1	120	27	5
Sb	0.4	0.4	0.4	0.4	0.4	0.4	0.4	0.4	0.4	0.4	0.4	0.4	0.4	0.4	0.4
Cs	0.4	0.4	0.9	0.4	0.6	0.4	0.4	0.4	0.4	0.4	0.4	0.4	0.5	0.4	0.4
Ba	86	165	271	139	193	128	166	162	415	278	203	112	129	109	85
La	5.2	4.9	27.2	6.8	10.3	19.7	13.2	5.8	11.5	16	4.8	11.1	8.9	7.2	5.7
Ce	11.6	11.3	58.6	15.3	20.8	45.7	30.1	14	22.7	31.1	10.7	24	13.1	15	12
Pr	2.08	1.71	7.62	2.24	2.54	6.06	3.94	1.97	2.64	3.87	1.44	3.01	2.09	2	1.5
Nd	11.3	8.6	32.2	11.4	10.3	26.6	19	10.5	11.8	17.6	7.7	13.5	8.9	10	6.6
Sm	3.9	3.2	7.4	3.6	2.6	6.6	5.1	3.4	3.1	4.4	2.3	3.3	2.6	3.2	2.1
Eu	1.39	1.27	2.3	1.33	0.87	2.25	1.88	1.19	1.13	1.38	0.87	1.21	0.9	1.2	0.7
Gd	4.6	3.9	6.9	6	3.2	6.5	5.4	4	3.9	4.7	2.8	3.5	3.5	3.9	2.6
Tb	0.7	0.7	1.1	0.7	0.6	1	0.9	0.6	0.6	0.8	0.5	0.5	0.6	0.7	0.5
Dy	7	3.8	6	4	3.5	5.7	4.9	3.9	7	7	2.8	3.2	3.8	6	3.1
Ho	0.8	0.7	1.1	0.8	0.7	1	0.9	0.8	0.9	0.8	0.6	0.6	0.8	0.8	0.6
Er	2.1	2	3.1	2.1	2	2.7	2.5	2.1	2.6	2.1	1.6	1.7	2.3	2.2	1.8
Tm	0.29	0.28	0.44	0.28	0.29	0.38	0.34	0.3	0.38	0.29	0.23	0.24	0.33	0.3	0.3
Yb	1.9	1.7	2.7	1.8	2	2.3	2	1.9	2.5	1.8	1.5	1.4	2.1	1.9	1.8
Lu	0.29	0.25	0.4	0.27	0.29	0.35	0.3	0.28	0.39	0.27	0.21	0.21	0.3	0.3	0.3

Hf	2.6	2	4.4	2.5	1.8	6	3.4	2.3	2	2.3	1.5	2.2	1.6	2.2	1.3
Ta	0.1	0.1	1.3	0.1	0.2	1.6	1	0.1	0.1	0.6	0.1	0.7	0.1	0.1	0.1
W	1	1	1	1	1	1	1	1	1	1	1	1	1	1	1
Tl	0.1	0.1	0.1	0.1	0.1	0.1	0.1	0.1	0.1	0.1	0.1	0.1	0.1	0.1	0.1
Pb	5	4	5	4	4	4	4	4	4	6	4	4	4	4	4
Bi	0.3	0.3	0.3	0.3	0.3	0.3	0.3	0.3	0.3	0.3	0.3	0.3	0.3	0.3	0.3
Th	0.8	0.9	4.1	1.4	2.2	1.9	1.2	1.2	2.7	3.3	1.1	1.1	1.7	1.4	1.6
U	0.1	0.1	1	0.1	0.3	0.5	0.3	0.1	0.2	0.3	0.1	0.3	0.3	0.1	0.3

Major element variations

Major elements which showed good linear correlations with SiO_2, $R \geq 0.75$, are MgO (-0.8723) and K_2O (0.7751), whereas those which showed moderate linear correlation with SiO_2, $0.75 > R \geq 0.5$, are Na_2O (0.6141) and Al_2O_3 (0.5215). The rest that included; Fe_2O_3 (-0.3948), CaO (0.2708), TiO_2 (-0.2502) and P_2O_5 (0.3931), exhibited poor linear correlation with SiO_2 (Figure 8). Major elements which showed good linear correlation with MgO (+ve and −ve) of $R \geq 0.75$ are K_2O (-0.7198) and Na_2O (-0.8728), whilst those which exhibit moderate correlation of $0.75 > R \geq 0.5$ are Al_2O_3 (-0.5166), TiO_2 (-0.5265) and P_2O_5 (-0.5777). The rest, apart from SiO_2 which is already reported above, that included; Fe_2O_3, MnO and CaO showed no correlation (Figure 9)
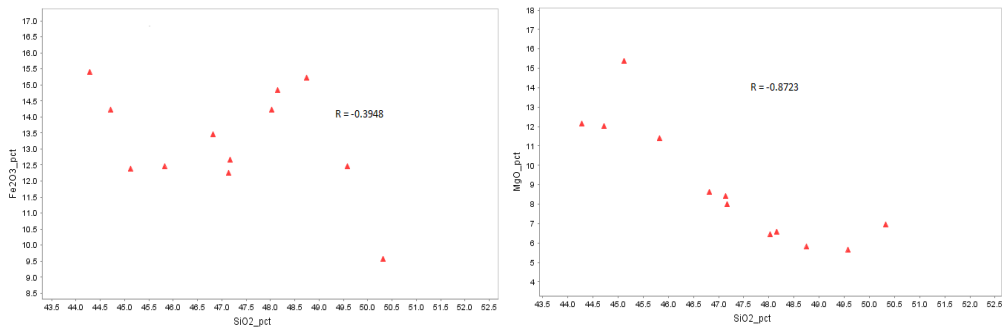

Figure 8: SiO_2 variation plots for some major oxides (in percentage weights) (R = Pearson linear correlation coefficient factor).
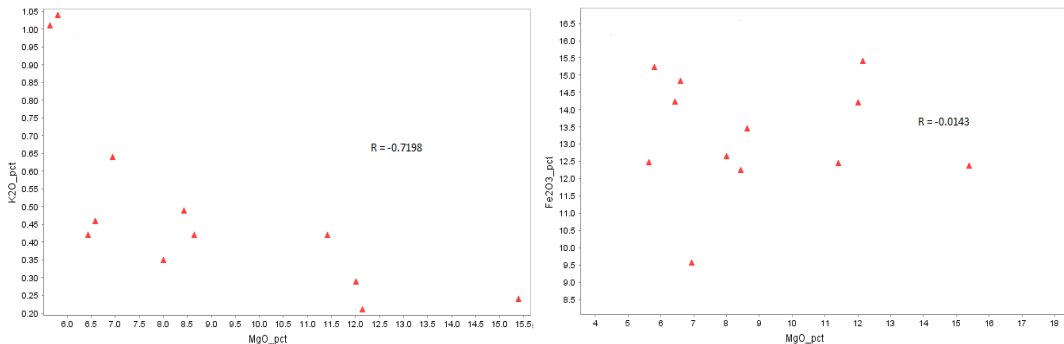

Figure 9: MgO variation plots for some of the major oxides (R = Pearson linear correlation coefficient factor).

Trace element variations

Three main compatible trace elements, Ni, Cr and Co, vary widely as follows: Ni, 80 to 720 ppm; Cr, 150 to 1400 ppm; and Co, 43 to 84 ppm. Selected incompatible trace

elements also showed wide content variation and these included: Sr, 91 to 325 ppm; Rb, 6 to 41 ppm; Nb, 2 to 23 ppm; Y, 17 to 29 ppm; Hf, 1.3 to 4.4 ppm and Th, 0.8 to 4.4 ppm. The compatible trace elements showed good correlation with MgO; with R values of 0.931, 0.9115 and 0.9039 for Ni, Cr and Co respectively (Figure 10). MgO was moderately negatively correlated ($0.75 > R \geq 0.5$) with incompatible trace elements; Sr, Zr, Nb andNd(Figure 11).
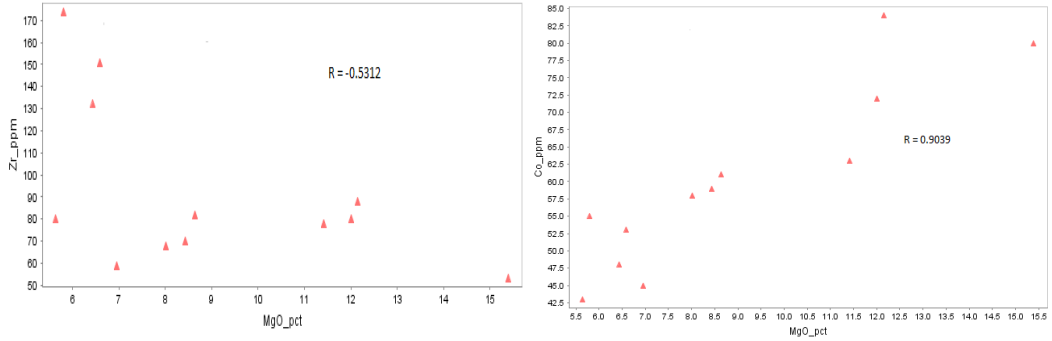

Figure 10: MgO versus some compatible trace elements variation diagram plots (R = Pearson linear correlation coefficient factor).
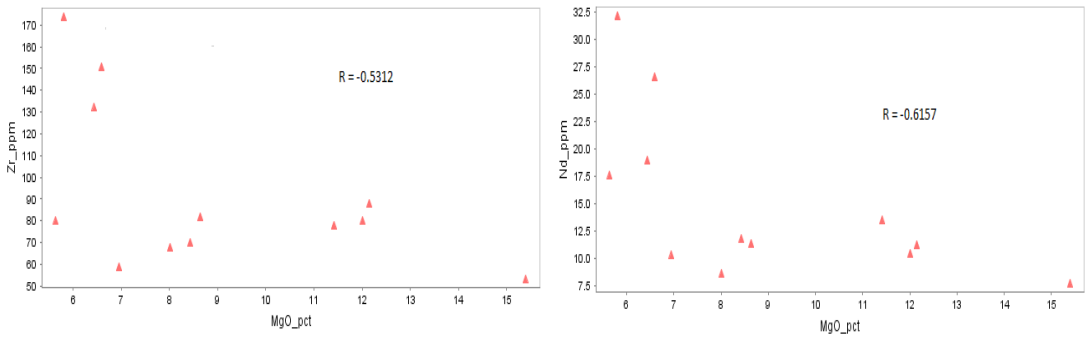

Figure 11: MgO versus some incompatible elements variation diagram plots (R = Pearson linear correlation factor).

Zr showed good correlation (R>0.75) with incompatible trace elements, Nb, La, Nd and Sm (Figure 12). In general, High Field Strength Elements (HFSE) and Rare Earth Elements (REE), exhibited good correlations with fractionation indices, MgO and Zr.
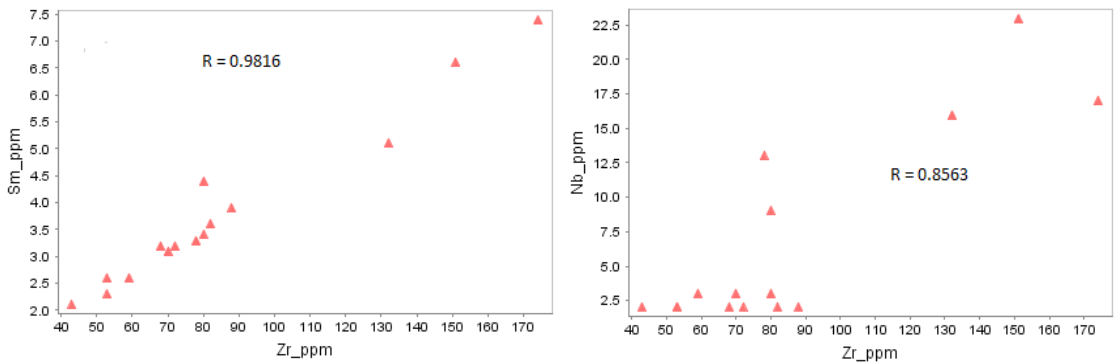

Figure 12: Zr versus some immobile elements variation diagram plots (R = Pearson linear correlation factor).

Geochemical classification of rocks

On the Cox *et al.* (1979) TAS model diagram all the samples were plotted in the Gabbro field apart from one outlier that had the lowest total alkalis (Figure 13). On the Irvine and Baragar(1971) model, the rocks plotted in sub-alkalic field (Figure 14a). On the Miyashiro (1974) SiO_2 vs FeO/MgO model of classification diagram, the samples showed that they are a mixture of tholeiitic and calc-alkalic suites (Figure 14b).
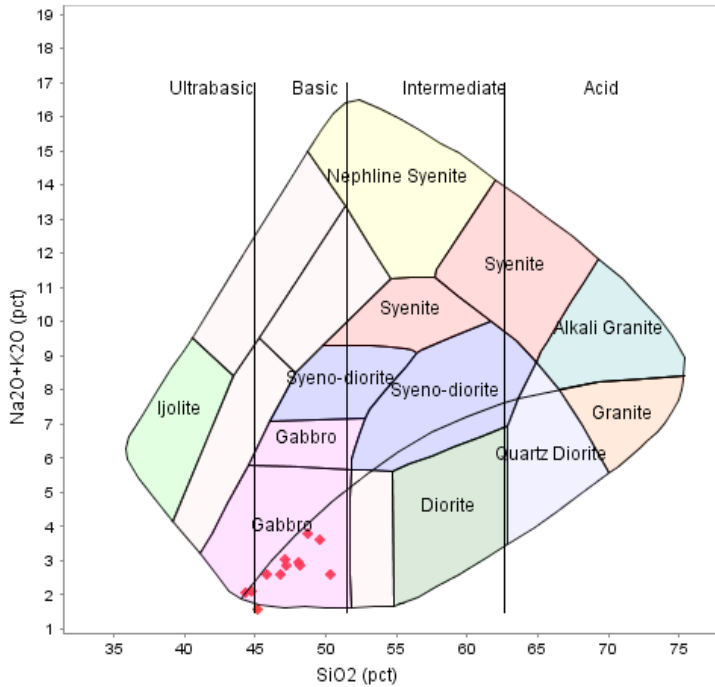
Figure 13: TAS Plutonic plots of the mafic dyke samples of the northeastern part of the Irumide Fold Belt, northeastern Zambia, diagram of Cox *et al.* (1979) adapted by Wilson (1989).

Figure 14: (a) Volcanic alkaline–subalkaline classification curve (after Irvine and Baragar, 1971); and (b) SiO2 vs FeO/MgO classification plot (after Miyashiro 1974, in Murphy *et al.* 2019) of the samples of the mafic dykes of the northeastern part of the Irumide Fold Belt, northeastern Zambia.
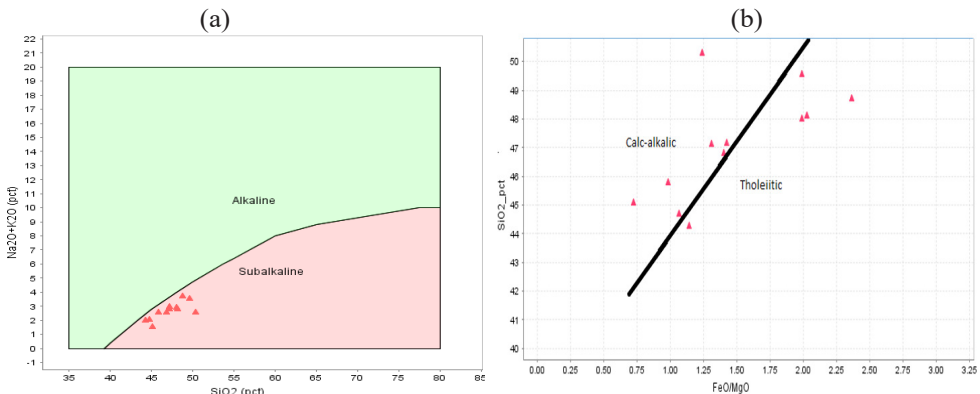
Rare earth elements geochemistry

In figure 15, the REE of both types of dykes, the calc-alkalic and tholeiitic, are plotted in variation diagrams which are chondrite-normalised to values of McDonough and the Sun (1995). The Chondrite-normalised REE diagram for tholeiitic rocks shows sub-parallel trends with elemental concentrations ranging between 8 to 120 times those of chondrite (Figure 15). Calc-alkalic rock samples did not display sub-parallel trends on the Chondrite-normalised REE diagram, but had elemental concentrations ranging between about 8 to 48 times those of chondrite. The diagrams showed that both types of mafic rocks, tholeiitics and calc-alkalics, were strongly enriched in the light REE (LREE) over the heavy REE (HREE). In the tholeiitic rocks, LREE enrichment of La, which was the most enriched, ranged between 50 to 120 times more enriched than the chondrite concentrations whilst Lu, which was the least enriched of the HREE ranges between 8 to 18 more enriched than the chondrite concentrations. In the calc-alkalic type of basalts, LREE were moderately enriched with La, the most enriched, ranging between 20 to 48 times more enriched than chondrite concentrations. The enrichment of the HREE was similar to that of the tholeiitic rocks. The LREE trend had a steeper slope to the right whilst HREE exhibited a relatively flat trend.
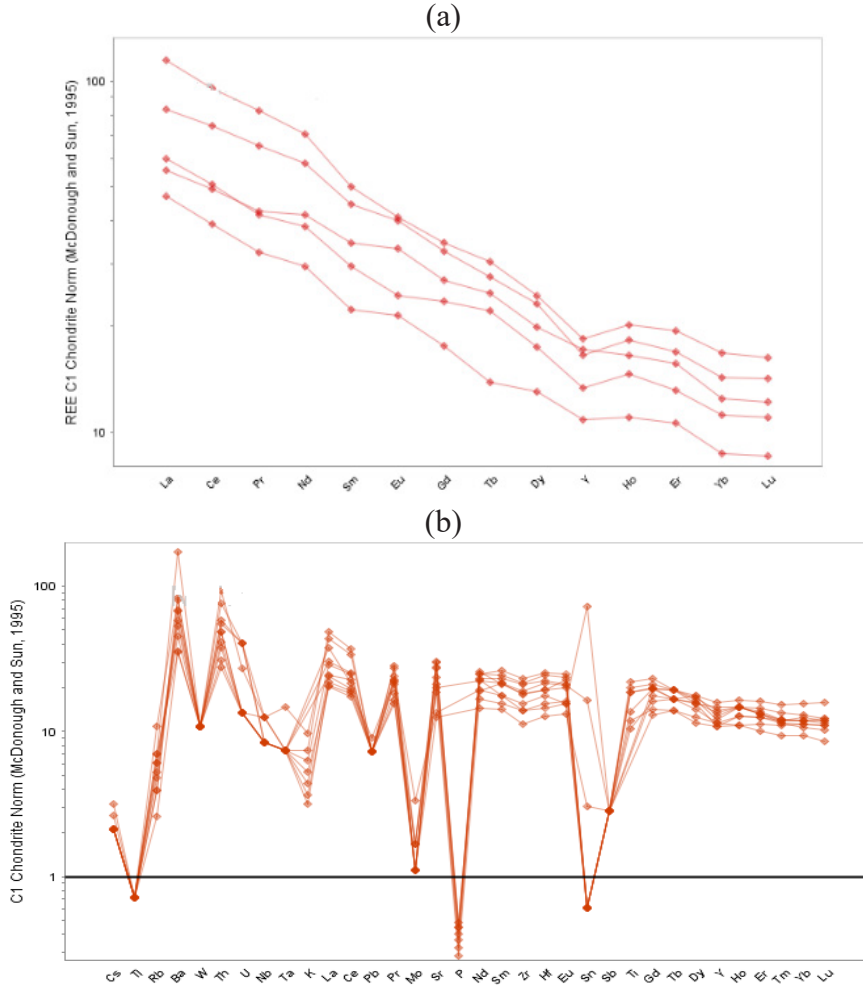
(a)

(b)

Figure 15: (a) Chondrite-normalised REE plot for tholeiitic rocks, and (b) Chondrite-normalised REE plot for calc-alkalic rocks of the Study area, normalising values from McDonough and Sun, 1995).

On the McDonough and Sun (1995), the chondrite-normalised multi-element variation diagrams, both types of dykes displayed strong negative anomalies for HFSE that included P, W and Pb; and weakly negative anomalies in the other HFSE such as Nb, Zr and Hf (Figure 16). The LILE displayed positive Ba and Sr anomalies but negative K anomalies. A strong positive correlation between Zr and REE is observed, especially in the LREE, which are more incompatible (Figure 17). On the primitive mantle-normalised multi-element spider diagram plot, of the calc-alkalic dyke samples studied, Pb showed a positive anomaly whilst Ti, Ta, Nb displayed troughs. The primitive mantle-normalised multi-element spider diagram plot for the tholeiitic dyke type samples did not display any significant anomalies in the elements displayed by the calc-alkalics(Figure 18).
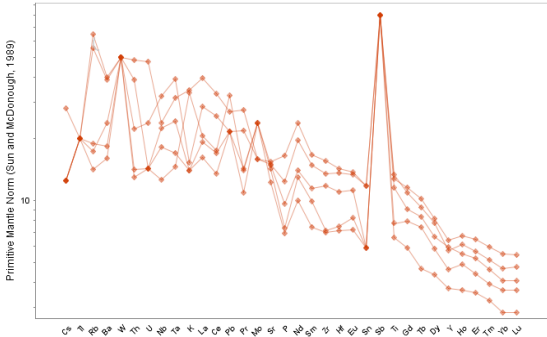
(a)

Figure 16: Chondrite-normalised ME variation diagrams for (a) tholeiitic dykes, and (b) calc-alkalic dykes of the study area, normalising values from McDonough and Sun, 1995).
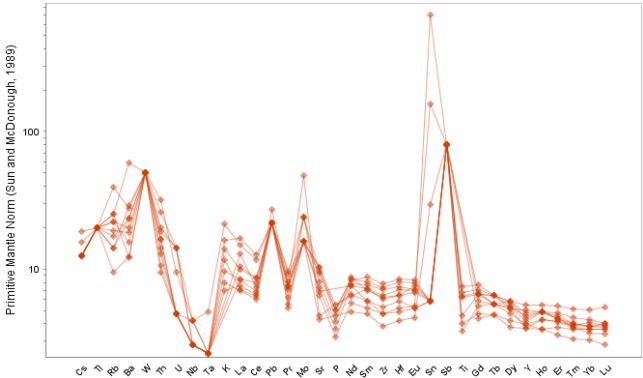

Figure 17: Zr vs REE, Sm and Nd, variation diagram plots (R = Pearson linear correlation factor)
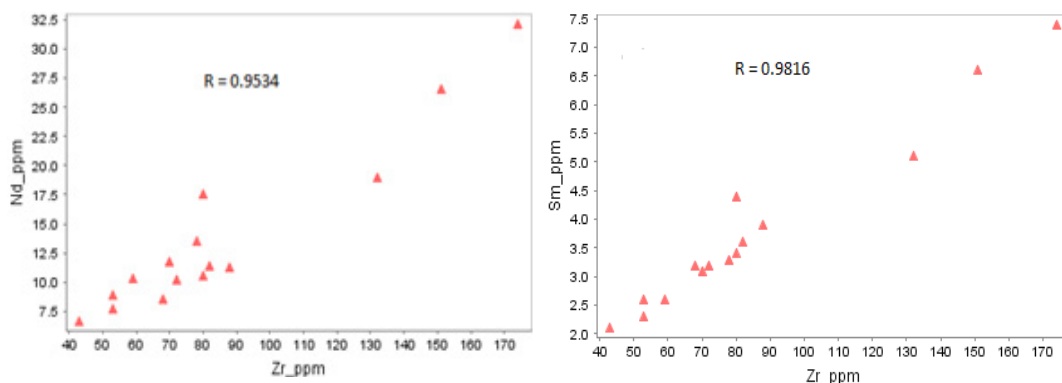
Figure 18: Primitive mantle-normalised multi element variation diagrams for (a) tholeiitic rocks, and (b) calc-alkalic rocks of the study area, normalising values from Sun and McDonough 1989. The plots show that the tholeiitic rocks are more evolved that the calc-alkalic rocks.

Isotope geochemistry and age dating

The measured ratios and ages of the analysed samples are shown in Tables 2 to 4 and the most useful information is summarised in Table 5. From these tables, it is observed that measured $^{87}Sr/^{86}Sr$ ratios (which measures the Sr isotopic ratio of a sample at the time of intrusion) fall within the narrow range of 0.710886-0.719612 (Table 2), whilst measured $^{143}Nd/^{144}Nd$ ranges between 0.512139-0.512370 (Table 3). The ages of the three dated samples are markedly different, being 608 ± 35 Ma, 1067 ± 55 Ma and 1522 ± 90 Ma (Table 4).

Table 2: Rb-Sr isotope ratios

Sample	Rb, ppm	Sr, ppm	$^{87}Rb/^{86}Sr$	±2σ	$^{87}Sr/^{86}Sr$	±2σ
CH-ISO-01	12.9	104	0.3591	0.0017	0.714503	0.000012
CH-ISO-02	16.0	154	0.3006	0.0015	0.710886	0.000010
CH-ISO-03	17.7	99	0.519	0.002	0.719612	0.000011

Table 3: Sm-Nd isotope ratios

Client's ID	K, % ± σ	^{40}Ar rad, (ng/g)	% ^{40}Ar air	Age, Ma	Error 2σ
CH-ISO-01	0.240±0.01	39.78±0.12	5.3	**1522**	90
CH-ISO-02	0.276±0.01	27.85±0.09	5.7	**1067**	55
CH-ISO-03	0.348±0.01	17.47±0.05	4.9	**608**	35

Table 4: K-Ar age dating results

Sample	Sm, ppm	Nd, ppm	$^{147}Sm/^{144}Nd$	±2σ	$^{143}Nd/^{144}Nd$	±2σ	εNd*
CH-ISO-01	2.449	8.298	0.1784	0.0005	0.512216	0.000009	-8.23
CH-ISO-02	3.112	9.880	0.1904	0.0005	0.512370	0.000007	-5.23
CH-ISO-03	1.990	6.664	0.1805	0.0005	0.512139	0.000004	-9.73

* - modern values

Table 5: Consolidated summary of isotopic and age data of the three samples of the study area

Sample No.	$^{87}Sr/^{86}Sr$	$^{143}Nd/^{144}Nd$	εNd	Age (Ma)
CH-ISO-01	0.714503	0.51226	-8.23	1522 ± 90
CH-ISO-02	0.710886	0.51237	-5.23	1067 ± 55
CH-ISO-03	0.719612	0.512139	-9.73	608 ± 35

Tectonic classification of the dykes

On the Pearce (2014) Th/Yb vs Nb/Yb discrimination plot (Figure 19a), the calc-alkalic samples plot in the overlap (transition) between Continental Arcs and Oceanic Arcs, which agrees with the geochemical data that shows significant evolution for the suite of the dykes. The dated samples, CH-ISO-01 to CH-ISO-03, are all calc-alkalic and plot in the same overlap between Continental Arcs and Oceanic Arcs (Figure 19b). On the same discrimination diagram of Th/Yb vs Nb/Ybby Pearce (2014)(Figure 19c), three of the 5 tholeiitic rock samples with the highest Nb/Yb ratio of all the samples plot in the E-MORB (Enriched Mid-Oceanic Ridge Basalt) field, but moving in the direction of the OIB (Oceanic Island Basalt) field. One sample with the lowest Nb/Yb ratio plots in the in the Continental Arcs field, and one plots at the region of Continental Arcs margin.
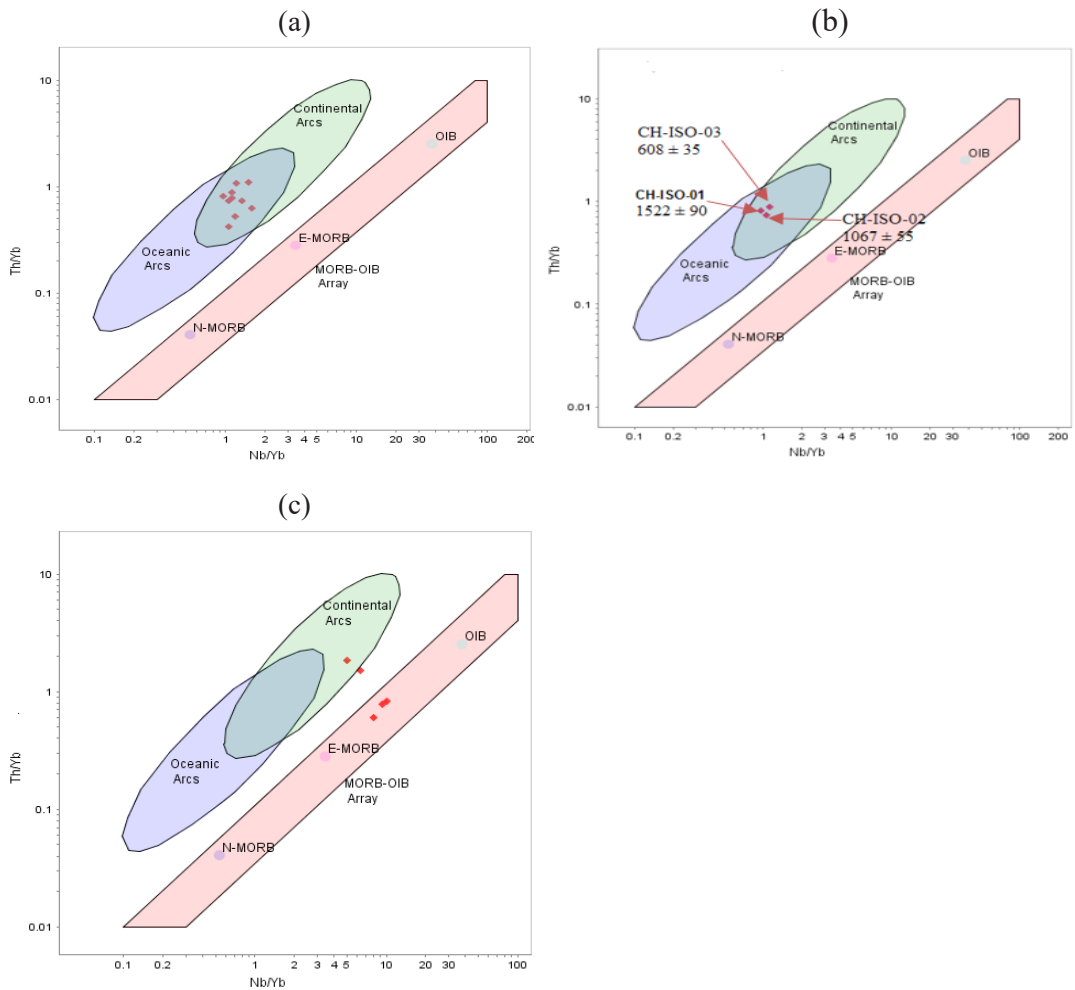
(a)

(b)

(c)

Figure 19: Diagrams of Basalt plot, Th/Yb vs Nb/Yb (Pearce 2014) geotectonic environment classification, (a) for all the calc-alkalic rocks; (b) for dated rock samples; and (c) for the tholeiitic rocks of the mafic dykes of the northeastern part of the Irumide Fold Belt, Zambia.

Discussion

Petrography

Information extracted from the examination of thin sections of any rocks being studied; igneous, metamorphic or sedimentary, complement hand-specimen observations. In this study, detailed petrographic analyses of twelve dyke swarm samples revealed that the mineralogical composition of the dyke rocks is composed of plagioclase, pyroxene, hornblende with subordinate olivine, sericite, epidote and opaque minerals. This mineral assemblage qualified the rocks to be classified as gabbroic.

Epidote was markedly more in the two of the four medium grained samples and exhibited subhedral to euhedral crystals, where it appeared to have totally replaced hornblende (see Figures 6C and D). In the same samples, hornblende also displayedsubhedral crystal texture. The crystal contacts of the two minerals were sharp, giving the impression that epidote did not replace hornblende from the edges. Hornblende

63

replacing olivine and augite indicated that some of the portions of the dykes could be classified as an alkaline olivine gabbro. The primary magmatic minerals included plagioclase, olivine, augite, and late brown hornblende (see Figure 5A). Probably very close to solidus temperatures, olivine and augite reacted with the hydrous residual liquid to grow hornblende rims on both of them (see Figure 7E). Imperfections in the augite possibly trapped liquid inclusions or exsolution lamellae (see Figure 7E), also reacted to grow hornblende within augite crystals. It was clearly observed that the hornblende rims were brown on augite and green on parts of the olivine (see Figure 6D).

Whole rock geochemistry

Igneous rocks seen on the Earth's surface originated by partial melting of a solid source in the mantle or sub-continent to produce primary magma and residual solid rock (De Paulo, 1981; Pearce, 1983; Turner *et al.*, 1997; Kelemen *et al.*, 2004; Esory *et al.*, 2010; Herzberg and Asimow, 2015). Once the magma is solidified, the rocks formed carry a chemical signature, similar to DNA in humans, of their source, processes of partial melting and all the other materials which interacted with them before solidification (Hanson, 1980). The chemical signature is preserved in their compositions for as long as there has been no significant post solidification alteration. By examining the chemical compositions of the specific unaltered rocks of interest, particularly trace element (which include REE) concentrations and their ratios, it is possible to determine the nature of the source region and the processes that took place during partial melting and ascent to emplacement.

In this study, petrogenetic processes which led to the emplacement of the dyke swarm rocks were assessed by the application of several chemical variation diagrams. Chemical variation diagrams are basically displays of element differences and trends which are shown by a related suite of rocks. Major elements were plotted against SiO_2, MgO and Mg#. The Mg# is used as an index to monitor the degree of fractional crystallisation that the magma exhibits, as it is insensitive to contamination (Cox, 1980). Higher values of Mg# indicate least evolved nature while the lower values are suggestive of fractionated nature of the concerned rocks (Karmalkar *et al.*, 2016). The calculated Mg# for the samples of this study, showed a wide variation with values ranging between 29.7 and 58.0. These Mg # numbers are much lower than the Mg# (70) estimated for primitive mantle-derived basaltic magmas (Halama *et al.*, 2004; Talusani, 2010; Cucciniello *et al.*, 2013).

The geochemical results of the dykes of northeastern Zambia, showed a range of SiO_2 (44. 24-50.32 wt%) over the ratio of FeO(T)/MgO. This is considered to be quite narrow and a feature that is typical of tholeiitic differentiation (Atherton and Ghani, 2002; Murphy *et al.*, 2019). The medium to high concentrations of Mg (5.64 -15. 39 wt%), Ni (80 -720 ppm), Cr (160 – 1400 ppm), V (206 – 344 ppm) and Ba (85 – 415 ppm) are indicative of a mantle source (Atherton and Ghani 2002). The high average values of Na_2O/K_2O (5.2) and $Na_2O + K_2O$ (2.71) indicated further that the rocks were sodic. The ratio of $Al_2O_3/(CaO+Na_2O+K_2O)$ ranged between 1.02 and 1.34, and this was an exhibition of marginal peraluminous characteristics ($Al_2O_3 > (CaO + Na_2O + K_2O)$).

The low FeO(T)/MgO ratio (0.7 – 2.4) exhibited by the dyke mafic samples is typical of calc-alkaline suites (Murphy *et al.*, 2019). The samples that were plotted in the tholeiitic field generally exhibited comparatively lower MgO and Mg#, but higher SiO_2, TiO_2 and P_2O_5, than the samples that were plotted in the calc-alkali field, an indication that they were more evolved. They also exhibited higher contents of Sr, Zr, Sm, Nd, La, Hf and Th. The same samples that were plotted in the tholeiitic field, further showed higher Ce/Yb and Nb/Yb ratios with a clear separation of the two types of rocks observed from Nb content, which was much higher in the tholeiites. The calc-alkalic rocks were richer in compatible elements of Ni and Cr. The Zr content in the two types of dykes is so markedly distinguishable, averaging 123 ppm for tholeiitic samples and 71 ppm for calc-alkalic samples.

Isotope geochemistry and age dating

Isotopic ratios are useful in the characterisation of the mantle source regions from which the mafic rocks being studied were derived. This is because, owing to the negligible mass difference between the isotopes of an element, isotopic ratios are unaffected by partial melting and fractional crystallisation (Ciborowski, 2013). In this regard, the initial isotopic ratios of the mafic rock, when the parent magma was extracted from the mantle, will be the same as the isotopic ratio of the source region at the time of extraction (Hanson, 1980). Further, the isotopic ratios measured in a sample are a function of the initial isotopic ratios and the rock's age (Ciborowski, 2013). In these studied samples, there was no observed relationship between the initial $^{87}Sr/^{86}Sr$ and $^{143}Nd/^{144}Nd$ with ages of the dykes. The negative eNd and $^{87}Sr/^{86}Sr$ values shown in Table 4.4 indicated a continental or contaminated magma (De Paolo 1988; Kerr, 2015).

Classification of geotectonic environment

Basaltic rocks are formed in almost every tectonic environment and they are believed to be geochemically sensitive to the changes in plate tectonic frameworks (Halls, 1982; Pearce, 1983; Holm, 1985;Schandl and Gorton, 2002; Duggen *et al.*, 2005; Harangi *et al.*, 2007). Multi-element and REE patterns are applied extensively to understand and make these classifications (Pearce, 1983). To understand the tectonic and magmatic processes that led to the emplacement of the dykes, chemical signatures were applied on the results of the studied samples. Discrimination diagrams, using some major element oxides, rare earth and trace elements, were applied. Trace and rare earth elements that included; Th, Hf, Ta, Yb, Y, Nb, La and Zr were applied in the evaluation due to their particular usefulness in the studies of arc magmatism (e.g. Pearce and Peate, 1995; Schandl and Gorton, 2002; Cimen, 2016). Nb and Ta are particularly useful in that the two elements are depleted in the continental crust relative to other highly incompatible elements such as caesium, rubidium, thorium, and uranium, and the light REEs, including cerium and lanthanum (Kelemen *et al.*, 1993). The discrimination diagrams applied on the selected elements revealed that the dyke suite was deposited in a back arc rift basin of a continental subduction environment.

Petrogenesis

Crustal contamination

In a situation where the mafic dyke rocks being studied are emplaced in a continental setting, like the study area, it is necessary to make an assessment of possible crustal contamination of the magma, before petrogenetic evaluations are carried out (e.g. Xiao *et al.*, 2004; Srivastava *et al.*, 2014; Kamalkar *et al.*, 2016). It is generally considered that when continental basaltic magmas rise from their sources in the mantle through the continental crust, they often experience contamination during ascent and or residence in crustal magma chambers (Watson, 1982, Halama *et al.*, 2004). The significance of crustal contamination can be assessed through correlations between indices of fractionation and the other chemical and/or isotope data of the rocks being studied (Tang *et al.*, 2012 and the references therein). In this study, for both dyke types, variation plots of MgO (as an index of fractionation) versus LILEs (Ba, Rb, Sr and K) and HFSEs (Ti, P, Zr, Y, Ce, Hf, Sm and Nd) were generated and analysed accordingly. The continental crust is largely felsic and any contamination of mafic magma is unlikely to alter the concentration of MgO, but will raise the concentration of most LILEs and HFSEs, which, because of their incompatibility, are more concentrated in these parts of the Earth. Uncontaminated mafic rocks will display more or less linear trends between MgO and the incompatible elements on variation plots, but display scatter if there is significant contamination. A combination of compatible and incompatible trace elements and their ratios, as well as isotope data, were also applied for this purpose (e.g. Rollinson 1993).

For tholeiitic dyke samples, on the variation plots against MgO (Figure 20), the LILEs; Ba, Rb, Sr and K; exhibited moderate to good negative correlation with linear coefficient factor ranging between -0.5717 to -0.9105. The HFSEs showed similar trends displayed by the LILEs (Figure 21). The trace element ratios of Nb/Y versus Zr/Y variation plot (Figure 22) yielded similar linear trend to those of MgO versus the LILEs and the HFSEs. Elemental ratios of the incompatible elements were, Zr/Nb = 6.0 - 10.24, Ba/La = 6.54 - 19.59, and Ba/Nb = 5.57 - 30.81. On the primitive mantle-normalised multi-element spider diagram plot of the tholeiitic rock samples (Figure 18b), no negative anomalies of Ta-Nb and Hf-Zr were noticed. The enrichment in LREE accompanied by flat HREE patterns, which is also a characteristic feature of crustally contaminated mafic rocks, are considered by Srivastava *et al.* (2014) as not being adequate to confirm crustal contamination. In summary, the studied samples of the tholeiitic mafic dykes of the Study area, do not show a clear indication of crustal contamination during the processes that led to their emplacement. The chemical characteristics exhibited by the analysed samples indicate that any suggestions of crustal contamination involvement during the magmatism of the tholeiitic rocks were clearly eliminated. If any contamination took place, it was insignificant.
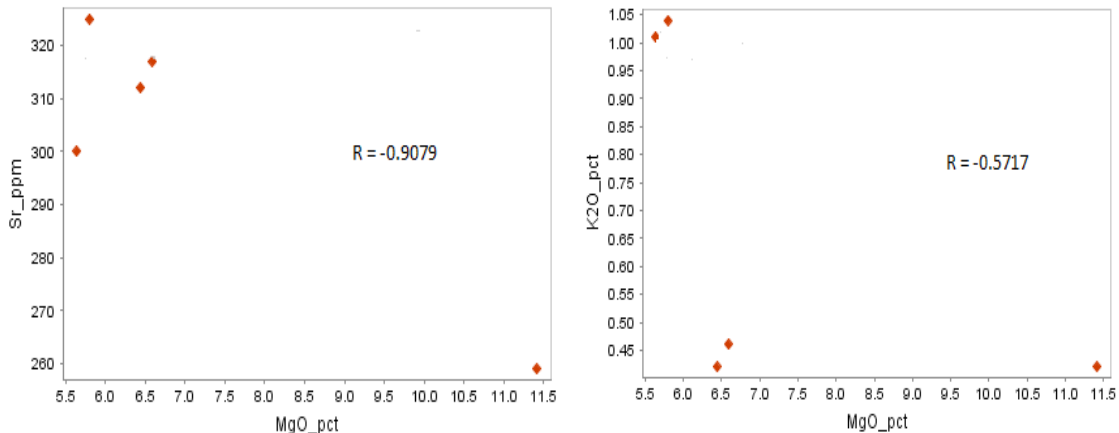
Figure 20: Variation plots of MgO versus some LILEs (incompatible elements), tholeiitic mafic dyke samples of the study area.
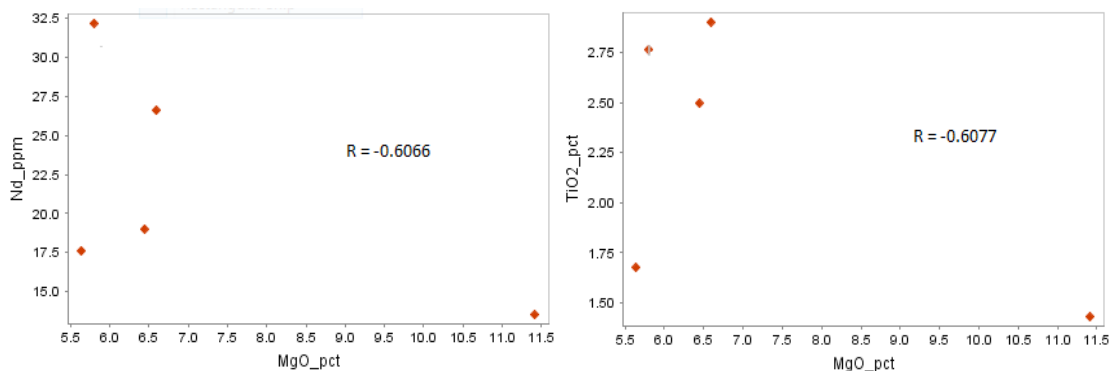

Figure 21: Variation plots of MgO versus some HFSE (incompatible elements), tholeiitic mafic dyke samples of the study area.
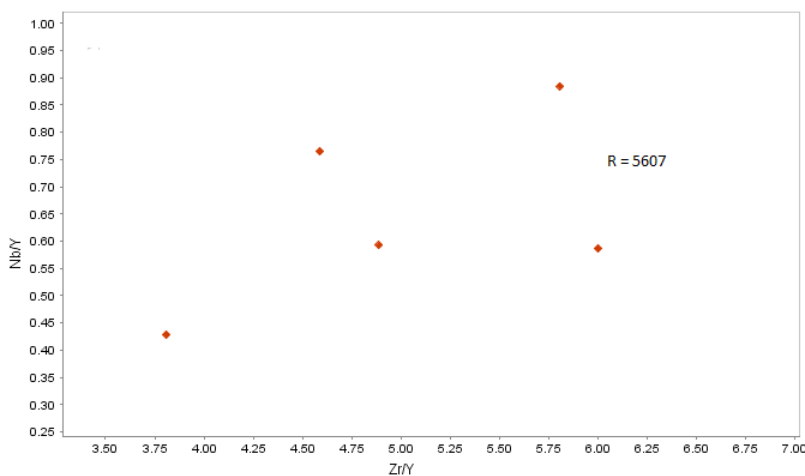

Figure 22: Variation plot of the ratios of Zr/Y versus Nb/Y, tholeiitic mafic dyke rock samples of the study area.

For calc-alkalic dyke samples, on the variation plots against MgO (Figure 23), the LILEs, Rb and K exhibited moderate to good negative linear trends, whereas Ba and Sr showed no correlation. The HFSEs (Figure 24) all showed negative, mostly very

poor, to no correlation with MgO. The trace element ratios plot of Nb/Y versus Zr/Y variation (Figure 25) showed absolutely no correlation to MgO.On the primitive mantle-normalised multi-element spider diagram plot of the calc-alkalic rock samples of the study area (Figure 18a), negative anomalies were noticed for Nb-Ta, whilst Hf-Zr showed no anomaly at all. On the primitive mantle-normalised multi-element spider diagram plot of the calc-alkalic rock samples of the study area (Figure 21), negative anomalies are noticed for Nb-Ta, whilst Hf-Zr show no anomaly at all. On the Chondrite-normalised REE variation diagram, the calc-alkalic dykes display a mild negative anomaly for Y. From the isotopic results of the three studied samples from the study area, which happens to all be calc-alkalic, the negative eNd(t) values (−5.23 to – 9.73) suggest contamination by crustal material. From the observed chemical characteristics, the studied samples of the calc-alkalic mafic dykes of the study area clearly indicate crustal contamination during the processes that led to their emplacement. There is also a possibility that the parent magma was drawn from a contaminated mantle melt.
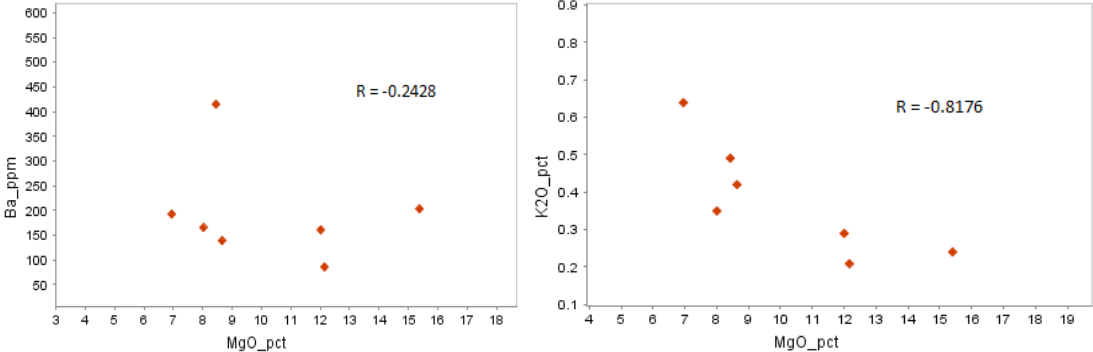

Figure 23: Variation plots of MgO versus some LILE (incompatible elements), calc-alkalic mafic dykes samples of the study area.
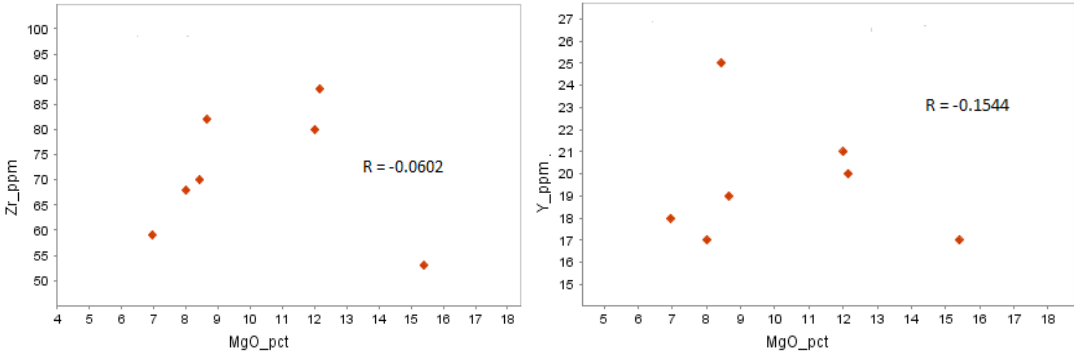

Figure 24: Variation plots of MgO versus someHFSE (incompatible elements), calc-alkalic mafic dykes samples of the study area
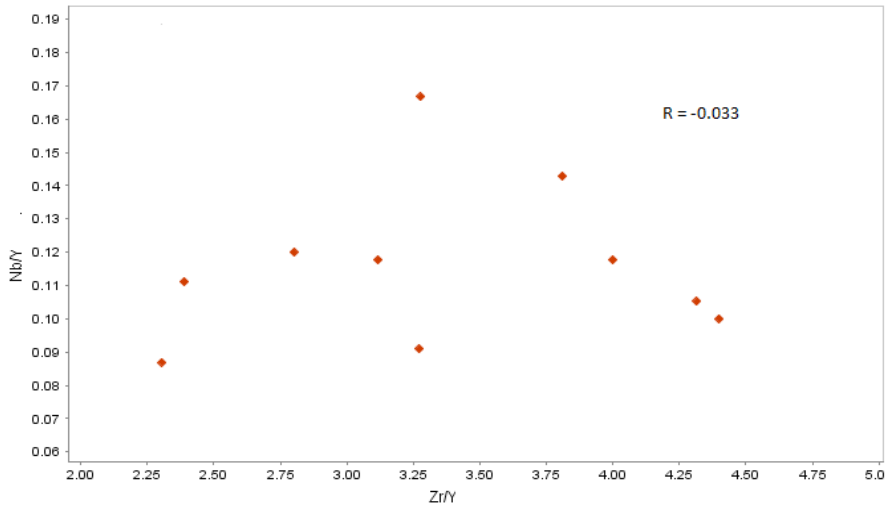
Figure 25: Variation plot of the ratios of Zr/Y versus Nb/Y, calc-alkalic mafic dyke rock samples of the Study area.

Fractional Crystallisation

The features observed in the results of the plots of different combinations, indicated specific information in fractional crystallisation processes. The observed decrease in MgO plus FeO(T) concentrations with the increase in SiO_2 indicates the crystallisation fractionation of olivine (Zi *et al.*, 2008), whilst the negative correlation between SiO_2 and CaO/Al_2O_3 suggested the clinopyroxene crystallisation fractionation. The decrease of compatible elements, Cr and Ni, with the decrease in Mg# (magma evolution) was indicative of the fractionation crystallisation of olivine and clinopyroxene (Zi *et al.*, 2008). The positive linear correlation between TiO_2 and P_2O_5 content indicated simultaneous fractionation from least differentiated mafic magma composition, with higher TiO_2-P_2O_5 content, to a more differentiated mafic magma that had lower TiO_2-P_2O_5 concentrations (Karmalkar *et al.*, 2016). The wide ranges of Mg#, MgO, Ni and Cr indicated significant crystallisation fractionation either in magma chambers or during ascent (Zi *et al.*, 2008; Srivastava *et al.*, 2014). The low Mg# (29.7 – 58.0), Ni (80–720 ppm) and Cr (150–1400 ppm) were suggestive of evolved magmas that underwent fractional crystallisation (Cheng *et al.*, 2015). Almost all the plotted major oxides increase with decreasing MgO, indicating crystallisation differentiation/fractionation (Figure 9). This fractional crystallisation is also evidenced by some variations exhibited in the results of decreasing elemental concentrations of TiO_2, CaO and P_2O_5, and the increase in the concentrations of SiO_2 (Figures 26 and 27).
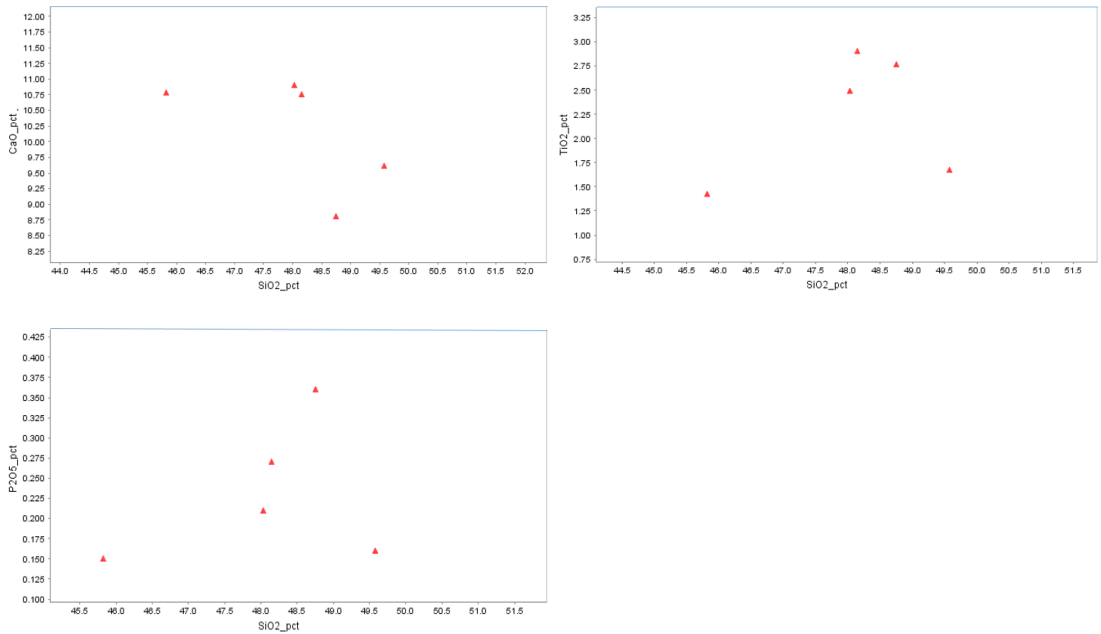
Figure 26: Variation plots of SiO2 vs CaO, TiO2 and P2O5, tholeiitic mafic dykes samples of the study area.
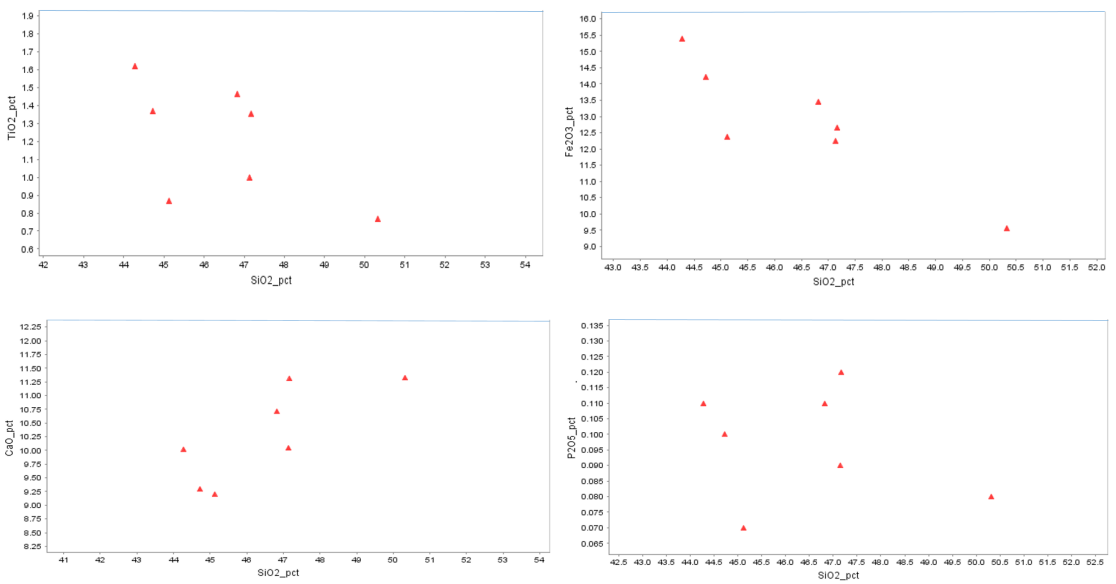
Figure 27: Variation plots of SiO2 vs CaO, TiO2, Fe2O3 and P2O5, calc-alkalic mafic dykes samples of the study area.

Magma source

An important integral part of any petrogetic studies of basaltic rocks is the evaluation of the source of the magma from which the rocks being studied crystallised, and in almost all cases, the source of the magma is the mantle (Takahashi, 1986; Pearce and Parkinson 1993; Turner and Hawkesworth, 1995; Phinney and Hall, 2001, Pertermann and Hirschmann, 2003a; Tatsumi and Suzuki, 2009; Srivastava *et al.*, 2014; Sreenivasulu

et al., 2014; Sayit *et al.*, 2016; Murphy *et al.*, 2019). Basaltic magmas possess inherent critical information about their mantle source chemical compositions. Continental basalts have several possible distinct mantle sources which include: 1) subcontinental lithospheric mantle (SCLM); 2) plume-related OIB (oceanic island basalt)-type mantle sources; and 3) depleted MORB (middle oceanic ridge basalt)-type asthenospheric mantle (Thompson *et al.*, 1984; Garfunkel, 2008; Tang *et al.*, 2012) (see Figure 28).
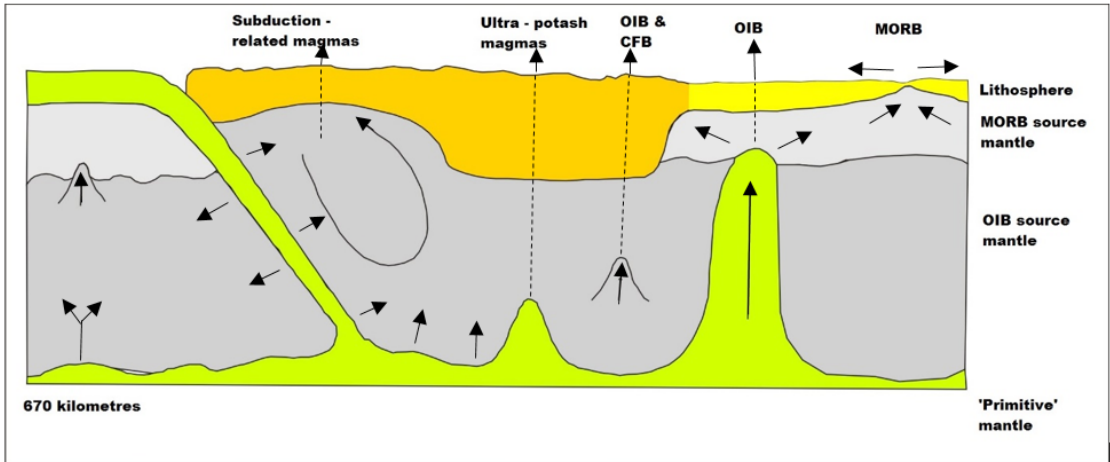

Figure 28: Sketch of model Upper Mantle circulation and magma genesis, modified from Thompson *et al.*, (1984).

Subduction-related magmas are generally considered MORB-OIB (generated within converting mantle wedges behind subduction zones) with complexities introduced by added components brought into the system through subduction (Thompson *et al.*, 1984; Stern, 2002; Manning, 2004; Savov *et al.*, 2007; Carlson *et al.*, 2018). In this process, subduction-zone fluids have played a substantial role in transferring typical slab-derived signatures from oceanic basalt and seafloor sediments to the mantle wedge (Yang *et al.*, 2012; Zhao *et al.*, 2013).

Partial melting and magma mantle source

The marked difference between calc-alkalic and tholeiitic magmas is the distinction in their major element contents and this has been suggested to be a product of both conditions of melting and variability in the composition of the sources of the two magma types (Takahashi and Kushiro, 1983; Takahashi, 1986; Kinzlerand Grove, 1992; Gaetani and Grove, 1998; Grove *et al.*, 2003; Munker *et al.*, 2004; Carlson *et al.*, 2018). Tholeiitic primary magmas are produced by the partial melting of dry peridotites (Jaques and Green, 1980; Fuji and Scarfe, 1985; Kinzler and Grove, 1992; Carlson *et al.*, 2018). Calc-alkalic primary magmas, on the hand, show evidence of melting of peridotites with high water contents (Carlson et al, 2018 and references therein). The high water concentrations, and distinctive trace element signatures that often include enrichment in fluid-mobile elements and depletion in high-field-strength (HFSE) trace elements, of primary calc-alkalic magmas, are often attributed to the melting of sources that

experienced some degree of metasomatism by fluids/melts released from subducting oceanic plates (Carlson *et al.,* 2018 and references therein).

The large difference in LILE/HFSE ratios between the tholeiitic and calc-alkalic dykes may reflect the difference in the abundances of these elements in the source regions rather than the degree of melting or processes of melting of compositionally similar sources (Carlson *et al.*, 2018). Therefore, the pattern observed from comparing the enrichment of LILE elements of the two types of dykes of the northeastern part of the Irumide Fold Belt, northeastern Zambia, was likely to represent both the pattern and degree of incompatible element compositional difference between their sources.

On the mantle source discrimination diagrams, eNd vs Th/Yb and eNd vs Ce/Yb, both of De Paolo (1988), (Figures 29(a) and 29(b) have all the three samples of the study area, which were analysed for isotopic data, plotted in the zone of Paleoproterozoic crust on both diagrams. Models of Gribble *et al.*, (1998) and Sayıt *et al.*, (2016) of TiO_2 vs Yb and Sm vs Sm/Yb respectively (Figure 30) showed that the samples analysed are products of partial melting that ranged about 5 to 20 per cent.
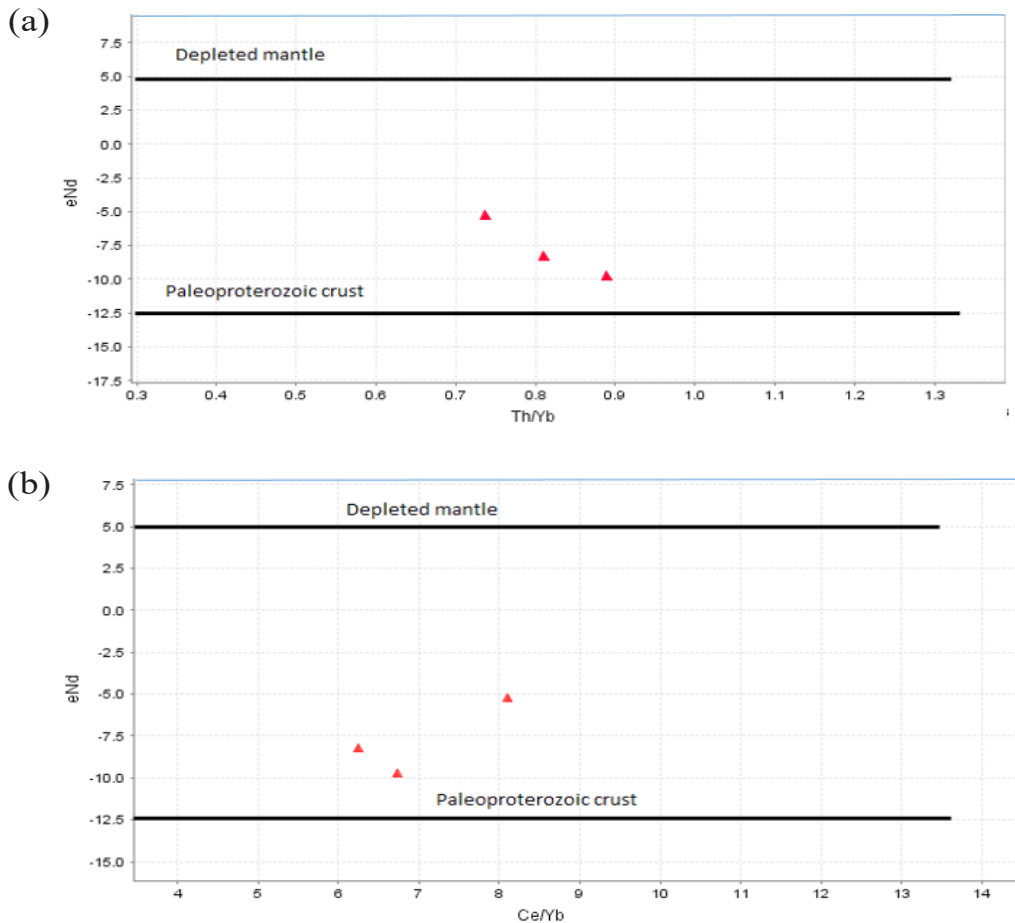
Figure 29: Isotope mantle source discrimination plots, (a) eNd vs Th/Yb, and (b), eNd vs Ce/Yb for the calc-alkalic dykes of the northeastern part of the Irumide Fold Belt, northeastern Zambia, after model diagrams of De Paolo (1988).

72

Figure 30: (a) Plot of TiO2 vs Yb, after Gribble *et al.*, (1998), and (b) Plot of Sm vs Sm/Yb, after Sayıt *et al.* (2016); partial melting diagrams for the Primitive Mantle calc-alkalic dykes of the Irumide Fold Belt of northeastern Zambia, adapted from Cimen, (2016).

Tectonic and geodynamic model

Figure 31: The tectonic and geodynamic model illustrating the development of the Irumide Rift Basin and emplacement of the mafic dykes:

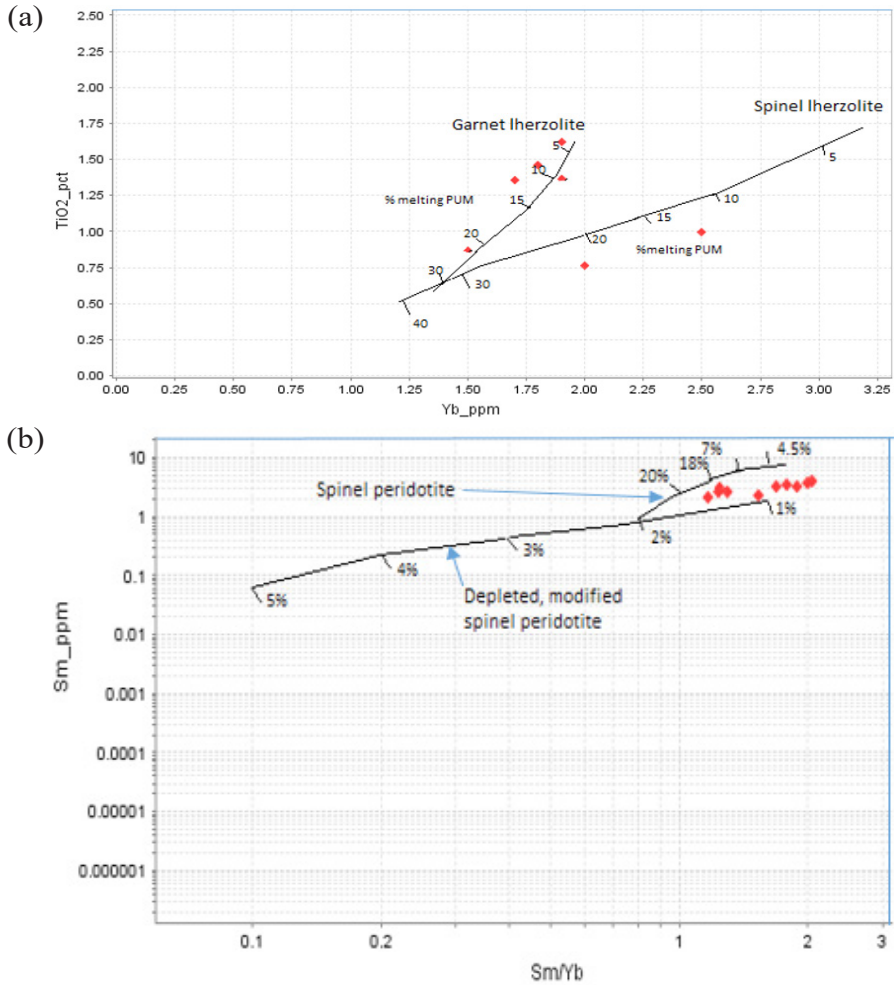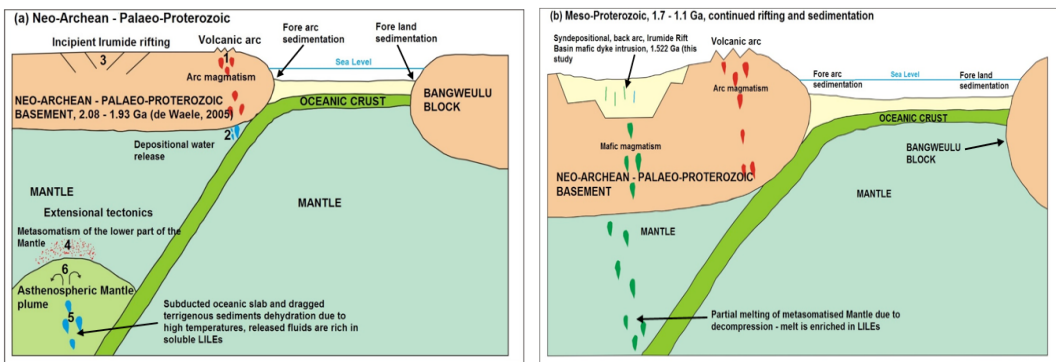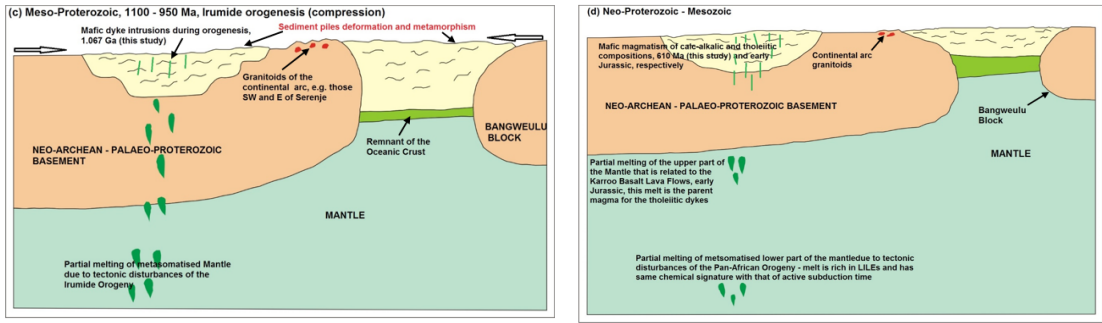(a) Neo-Archean – Palaeo-Proterozoic; 1. Continental magmatic arc rocks established at 1.87 and 1.82 Ga (De Waele and Fritzsimmons, 2007); 2. Release of depositional water from terrigenous sediments dragged down by the subducted oceanic slab, hot fluids lower the melting temperature in the continental crust as it moves up, triggering partial melting resulting in continental arc magmatism; 3. Incipient back arc Irumide rifting induced by asthenospheric mantle plume which caused extensional tectonics – started probably about the same time with the oldest magmatic arc rocks emplacement at about 1.85 Ga; 4. Metasomatism of the lower parts of the mantle by hot fluids derived from dehydration of the oceanic slab and dragged terrigenous sediments due to very high temperatures. The fluids are rich in soluble LILEs and poor in insoluble HFSEs; 5. Oceanic slab and terrigenous sediments dehydration; and 6. Development of asthenospheric mantle plume due to interaction of the Mantle material with dehydration fluids;

(b) Meso-Proterozoic period of extensional tectonics and sediment filling of the Irumide back arc rift basin followed by rifting induced decompression resulting in partial melting of the metasomatised Mantle thereby generating magma of the calc-alkalic dykes intruded at about 1.522 Ga (this study);

(c) Meso-Proterozoic, 1100 – 950 Ma, Irumide deformation and metamorphism (Daly, 2007), partial melting of the metasomatised lower parts of the Mantle due to tectonic disturbances (instigated by the break-up of the Rodinia Supercontinent) leading to the intrusion of calc-alkalic mafic dykes dated at about 1.067 Ga (this study); and

(d) Neo-Proterozoic – Mesozoic, partial melting of metasomatised lower parts of the Mantle due to tectonic disturbances of the Pan African Orogeny, giving rise to intrusion of calc-alkalic dykes dated at about 610 Ma (this study), whilst the upper parts of the Mantle, below the Irumide Rift fill, experienced partial melting associated with the Karoo continental flood basalts resulting in the intrusion of the tholeiitic dykes in early Jurassic (Mesozoic) (tholeiitic dykes have not been dated in this study).

CONCLUSIONS

From the study of the thin sections and photomicrographs, it has been concluded that the dykes studied were gabbroic in composition and exhibited differences in composition, textures, alteration and microstructures. They were composed mainly of plagioclase, clinopyroxene, hornblende with subordinate olivine, quartz, sericite, epidote and opaque phase minerals. The dyke rocks occured mainly as coarse and medium grained varieties because only two of the twelve samples examined, were fine grained. Relict igneous textures indicate that plagioclase was preferentially subhedral in some thin sections, with grain boundaries between plagioclase and clinopyroxene usually being cuspate. This is a sure sign of high temperature deformation processes as grain boundaries diffused to volume diffusion. Brittle deformation was predominant in some samples where plagioclase is more cracked than clinopyroxene. The brittle deformation was likely to have been caused by later tectonic activities, probably the Karroo rifting, well after the rocks had cooled down.

Alteration in most of the dykes samples was observed to primarily occur along cracks and was observed in plagioclase grains and perimeter of mafic phase groups in thin section. Only minor alteration occurred within a cluster of mafic minerals and alteration of olivine was predominantly serpentinisation, primarily localised along fractures.

The geochemical data obtained from the calc-alkalic dykes of the dyke swarm of the north-eastern part of the Irumide Fold Belt, Zambia, confirmed that this part of the orogenic belt was deposited in a back arc rift basin of a continental subduction environment as reported by Daly (1986), and De Waele *et al.* (2006) (Figure 31). Sample number CH-ISO-01 with an age date of 1522 ± 90 Ma was deposited in this type of environment in the Mesoproterozoic; sample number CH-ISO-02 with an age date of 1067 ± 55 Ma was also deposited in the same type of environment in the Mesoproterozoic; whilst sample number CH-ISO-03 with an age date of 608 ± 35 Ma was deposited in the same type of environment in the Neoproterozoic (Figure 19b).

The dyke swarm occurs as a suite of a mixture of sub-alkaline tholeiitic and calc-alkalic individual dykes of variable dimensions.

Geochronological K-Ar dating revealed that the calc-alkalic mafic dykes were intruded in at least three pulses, 1522 ± 90 Ma, 1067 ± 55 Ma and 608 ± 35 Ma. The first phase of intrusion may be the group that was described by Page (1973) as the syn-rifting and deposition of the rift sediments in the Irumide Rift Basin. This was deformed and during the Irumide Orogeny. The second pulse that was given by the results happened during the extensional tectonics related to the breaking up of the Rodinia Supercontinent, around 1000 Ma, that led to global mafic magmatism. The third recorded pulse obtained from the age dating results happened during the Neoproterozoic Pan African compressional orogenic events.

The tholeiitic dyke intrusions postdate the Karoo sedimentation and these are related to the Batoka Basalts, which are the youngest in the Karroo stratigraphy. The age of the tholeiitic dykes are obtained from Page (1973), who described some of the dykes he mapped to be cutting through the Karroo sediments. The tholeiitic dykes were as a result of continental rifting and were not cogenetic to the calc-alkalic dykes.

The several diagrams which were applied in the evaluation of crystallisation fractionation

of both types of rocks revealed that fractional crystallisation affected the magma of both types of rocks studied, tholeiitics and calc-alkalics. This is further supported by the wide ranges of Mg#, MgO, Ni and Cr in both rock types, which indicate significant crystallisation fractionation either in magma chambers or during ascent.

Both types of dykes show enrichment of the source magma by addition. The enrichment must principally have come from the terrigenous felsic sediments rich in HFSE and LILE which were subducted at the mantle wedge.

References

Aldanmaz, E., Yalınız, M. K., Guctekin, A., and Goncuoglu, M. C., 2008. Geochemical characteristics of mafic lavas from the Tethyan ophiolites in western Turkey: implications for heterogeneous source contribution during variable stages of ocean crust generation, Geological Magazine, 145, pp. 37-54.

Arndt N. T., Lesher C. M., Czamanske G. K., 2005. Mantle-derived magmas and magmatic Ni-Cu-(PGE) deposits. Economic Geology, 100th Anniversary volume, pp. 5-24.

Atherton, M.P. and Ghani, A.A. (2002). Slab Breakoff: A Model for Caledonian, Late Granite Syncollisional Magmatism in the Orthotectonic (Metamorphic) Zone of Scotland and Donegal, Ireland. Lithos, 62, pp. 65-85.

Banno, S. and Matsui, Y., 1973. On the formulation of partition coefficients for trace elements distribution between minerals and magma. Chem. Geol. 11, pp. 1-15.

Cabanis, B. and Lecolle, M., 1989. The La/10-Y/15-Nb/8 Diagram: A Tool for Discrimination Volcanic Series and Evidencing Continental Crust Magmatic Mixtures and/or Contamination. CompteRendus de l'Academie des Sciences, Seris II, Mécanique, Physique, Chimie, Sciences de l'univers, Sciences de la Terre 309(20), pp. 2023–2029.

Caro, G. and Bourdon, B., 2010. Non-chondritic Sm/Nd ratio in the terrestrial planets: Consequences for the geochemical evolution of the mantle-crust system. Geochimica et CosmochimicaActa, Volume 74, Issue 11, pp. 3333-3349.

Chen, J. Y., Yang, J. H. and Ji, W. Q., 2017. Ages and petrogenesis of Jurassic and Cretaceous rocks in the Matsu Island: implications of the lower crust modification beneath southeast China. *Journal of Asian Earth Sciences* 150 (2017), pp. 14-24.

Cheng, Z., Zhang, Z., Hou , T., Santosh, M., Zhang, D. and Ke, S., 2015. Petrogenesis of nephelinites from the Tarim Large Igneous Province, NW China: Implications for mantle source characteristics and plume–lithosphere interaction. Lithos 220-223 (2015), pp. 164-178.

Ciborowski T. J. R., 2013. The Geochemistry and Petrogenesis of the Early Proterozoic Matachewan Large Igneous Province, unpublished PhD Thesis, Cardiff University, 461 pp.

Cimen, O., 2016. Petrology and geochronology of the igneous rocks from Cangaldag Metamorphic Complex and the Cangaldag Pluton (Central Pontides, Turkey). Unpublished PhD thesis, Middle East Technical University, 282 pp.

Costa, A., Melnik, O. and Sparks, R. S. J., 2007. Controls of conduit geometry and wallrock elasticity on lava dome eruptions. Earth and Planetary Science Letters 260, pp. 137-151.

Cucciniello, C., Choudhary, A.K., Zanetti, A., Sheth, H. C., Vichare, S. and Pereira, R., 2013. Mineralogy, geochemistry and petrogenesis of the Khopoli mafic intrusion, Deccan Traps, India. Mineralogy and Petrology (2013), vol. 108, pp. 333-351.

Daly, M. C., 1986. The tectonic and thermal evolution of the Irumide belt, Zambia. PhD Thesis, University of Leeds, Leeds, 326 pp.

De Paolo D. J., 1988. Neodymium Isotope Geochemistry. An Introduction. Springer-Verlag, Berlin, 187 pp.

De Waele, B. and Mapani, B., 2002. Geology and correlation of the central Irumide belt. *Journal of African Earth Sciences*, 35(3): pp. 385-397.

Fahrig, W.F., Christie, K.W., Chown, E.H., Janes, D., Machado, N., 1986. The tectonic significance of some basic dyke swarms in the Canadian Superior-Province with special reference to the geochemistry and paleomagnetism of the Mistassini Swarm, Quebec, Canada. Canadian Journal of Earth Sciences 23 (2), pp. 238–253.

Gaetani, G. A.; Grove, T. L. and Bryan, W. B., 1993. The influence of water on the petrogenesis of subduction-related igneous rocks. Nature 365, pp. 332-334.

Garfunkel, Z., 2008. Formation of continental flood volcanism - the perspective of setting of melting. Lithos 100, pp. 49-65.

Gribble, R. F., Stern, R. J., Newman, S., Bloomer, S. H., and O'Hearn, T., 1998. Chemical and isotopic composition of lavas from the northern Mariana Trough; implications for magma genesis in back-arc basins. Journal of Petrology, 39, pp. 125-154.

Halama, R., Marks, M., Brugmann, G., Siebel, W., Wenzel, T., and Mark, G., 2004. Crustal contamination of mafic magmas: evidence from a petrological, geochemical and Sr-Nd-Os-O isotopic study of the Proterozoic Isortoq dike swarm, South Greenland. Lithos 74 (2004), pp. 199-232.

Hall, H. C., 1982. The importance and potential of mafic dyke swarms in studies of geodynamic processes. Geological Society of Canada 9, pp.145-154.

Hanson, G. N., 1980. Rare Earth Elements in petrogenetic studies of igneous systems. Ann. Rev. Earth Planet. Sci. 1980, 8, pp. 371-406.

Harangi, S., Downes, H., Thirlwall, M. and Ling, K. G. M. E., 2007. Geochemistry, Petrogenesis and Geodynamic Relationships of Miocene Calc-alkaline Volcanic Rocks in the Western Carpathian Arc, Eastern Central Europe. *Journal of Petrology* Volume 48 Number 12, pp. 2261-2287.

Herzberg, C. and Asimow, P. D., 2015. PRIMELT3 MEGA.XLSM software for primary magma calculation: Peridotite primary magma MgO contents from the liquidus to the solidus. Geochem., Geophys., Geosyst., 16, pp. 563-578.

Holm, P. E., 1985. The geochemical fingerprints of different tectonornagmatic environments using hygromagmatophile element abundances of tholeiitic basalts and basaltic andesites – Chem. Geol., 51, pp. 303-323.

Irvine, T. N. and Baragar, W. R. A., 1971. A guide to the chemical classification of the common volcanic rocks. Canadian Journal of Earth Science, 8, pp. 523-548.

Lewington G. L. D., 1987. The Geology of the Chikwa and Lake Beu Area; Explanation of Degree Sheets 1132, SE Quarter and 1133, part of SW Quarter. Geological Survey of Zambia Report No. 62, 25 pp.

Karmalkar, N. R., Duraiswami, R. A., Jonnalagadda, M. K., Griffin, W. L., Gregoire, M., Benoit, M. and Delpech, G., 2016. Magma Types and Source Characterization of the Early Deccan Magmatism, Kutch Region, NW India: Insights from Geochemistry of Igneous Intrusions. Special Publication of the Geological Society of India No. 6, 2016, pp. 193-208.

Kelemen, P. B., Shimizu, N. and Dunn, T., 1993. Relative depletion of niobium in some arc magmas and the continental crust: partitioning of K, Nb, La and Ce during melt/rock reaction in the upper mantle. Earth and Planetary Science Letters 120 (1993), pp. 111-134.

Kelemen, P. B., Hanghoj, K. and Greene, A. R., 2004. One view of the geochemistry of subduction-related magmatic arcs, with an emphasis on primitive andesite and lower crust. In: Treatise on Geochemistry, Vol. 3: The Crust, ed. R. L. Rudnick, pp. 593–659.

Kerr, A. and Fryer, B.J., 1993. Neodymium isotopic evidence for crust-mantle interaction in the genesis of 'A-type' granitoid suites in Labrador, Canada. Chemical Geology, Volume 103, pp. 39-60.

Kerr, A., 2015. Sm-Nd isotopic geochemistry of rare earth element mineralisation and associated peralkaline granites of the Strange Lake Intrusion, Labrador. Current Research (2015), Newfoundland and Labrador Department of Natural Resources; Geological Survey, 15-1, pp. 63 – 83.

Lesher, C. M. and Keays, R. R., 2002, Komatiite-Associated Ni-Cu-(PGE) Deposits: Mineralogy, Geochemistry, and Genesis, in L. J. Cabri (Editor), The Geology, Geochemistry, Mineralogy, and Mineral Beneficiation of the Platinum-Group Elements, Canadian Institute of Mining, Metallurgy and Petroleum, Special Volume54, pp. 579-617.

Maurice, C., David, J., O'Neil J. and Francis, D., 2009. Age and tectonic implications of Paleoproterozoic mafic dyke swarms for the origin of 2.2 Ga enriched lithosphere beneath the Ungava Peninsula, Canada. Precambrian Research 174, pp. 163-180.

McCuaig, T. C. and Hronsky, J. M. A., 2014. The Mineral System Concept: The Key to Exploration Targeting, Society of Economic Geologists, Inc. Special Publication 18, pp. 153-175.

Miyashiro, A., 1971. Processes and patterns of metamorphism in a plate tectonic framework. Geological Society of America, Abstracts with Programs 3, 648 pp.

Munteanu, M., Wilson, A. H., Costin, G., Yao, Y., Lum, J. E., Jiang, S. Y., Jourdan, F., Chunnett, G., and Cioac, M. E., 2017. The Mafic–Ultramafic Dykes in the Yanbian Terrane (Sichuan Province, SW China): Record of Magma Differentiation and Emplacement in the Emeishan Large Igneous Province. Journal of Petrology, 2017, vol. 58, No. 3, pp. 513-538.

Murphy, J. B., Nance, R. D., Gabbler, L. B., Martell, A., and Archbald, D. A., 2019. Age, Geochemistry and origin of the ArdaraAppinite Plutons, Northwest Donegal, Ireland. Geoscience Canada Vol. 46 (2019), pp 31- 48.

O'Connor, E. A., 1976. Geology of the Lumezi River and Lundazi areas; Explanation of Degree Sheets 1232 NE Quarter and parts of 1233 NW and NE Quarters. Geological Survey of Zambia Report No.71, 29 p.

Page, T. C., 1973. The Geology of the Chama Area; Explanation of Degree Sheet 1133, NW Quarter. Geological Survey of Zambia Report No.57, 25 pp.

Pearce, J. A., Peate, D. W., 1995. Tectonic implications of the composition of volcanic arc magmas. Annual Review of Earth and Planetary Sciences 23, pp. 251–285.

Pearce, J. A., 1983. Role of the subcontinental lithosphere in magma genesis at active continental margins. In: Hawkesworth, C. J., and Norry, M. J. (eds), Continental basalts and mantle xenoliths. Shiva, Nantwich, England, pp. 230-249.

Pearce, T. H., Gorman, B. E. and Birkett, T. C., 1975. The TiO_2-K_2O-P_2O_5 diagram a method of discriminating between oceanic and non-oceanic basalts, Earth and Planetary Sciences Letters, 24, pp. 419-426.

Pearce, J. A. and Cann, J. R., 1973. Tectonic setting of basic volcanic rocks determined using trace element analysis. Earth Planet Sci. Lett. 19: pp. 290-300.

Phinney, W. C. and Hall, H. C., 2001. Petrogenesis of the Early Proterozoic Matachewan Dyke Swarm, Canada,, and implications for magma emplacement and subsequent deformation. Canadian Journal of Earth Sciences, 38, pp 1541-1563.

Sayit, K., Marroni, M., Goncuoglu, M.C., Pandolfi, L., Ellero, A., Ottria, G. and Frassi, C., 2016. Geological setting and geochemical signatures of the mafic rocks from the Intra-Pontide Suture Zone: implications for the geodynamic reconstruction of the Mesozoic Neotethys. *International Journal of Earth Science,* 105, pp. 39-64.

Schandl, E. S., and Gorton, M. P., 2002. Application of high field strength elements to discriminate tectonic settings in VMS environments. Economic Geology 97, pp. 629-642.

Sheraton, J. W. and Sun, S. S., 1997. Mafic dyke swarms of the western Musgrave Block, central Australia: theirgeochemistry, origin, and relationships to the Giles Complex. Journal of Australian Geology andGeophysics. 16(5), pp. 621-636.

Sial, A. N., Oliveira, E. P. and Choudhuri, A., 1987. Mafic Dyke Swarms of Brazil; in Mafic Dyke Swarms; Editors: Halls, H. C. and Fahrig, W. F. Geological Association of Canada Special Paper 34, pp. 467- 481.

Sreenivasulu, P., Padmasree, P., and Vijayakumar, K. S., 2014. Petrology, geochemistry and tectonic setting of mafic dyke swarms of Kadiri Schist Belt, Eastern Dharwar Craton, South India. *International Journal of Basic and Applied Chemical Sciences,* vol. 3, July-September, pp. 34 – 43.

Srivastava, R. K., Jayananda, M., Gautam, G. C. and Samal, A. K., 2014. Geochemical studies and petrogenesis of 2.21 – 2.22 Ga Kunigal mafic dyke swarm (trending N-S to NNW-SSE) from eastern Dharwar craton, India: implications for Paleo Proterozoic large igneous province and supercratonicsuperia. Miner Petrol (2014): 108, pp. 695 – 711.

Sun, S. S. and McDonough, W. F., 1989. Chemical and Isotopic Systematics of Oceanic Basalts: Implications for Mantle Composition and Processes. In: Saunders, A.D. and NorryM.J., Eds., Magmatism in the Ocean Basins, Vol. 42, Geological Society, London, Special Publications, pp. 313-345.

Talusani, R. V. R., 2010. Bimodal tholeiitic and mildly alkalic basalts from Bhir area,

central Deccan Volcanic Province, India: Geochemistry and petrogenesis. Journal of Volcanology and Geothermal Research 189 (2010), pp. 278–290.

Tang, G. J., Wang, Q., Wyman, D. A., Li, Z. X., Xu, Y. G. and Zhao, Z. H., 2012. Metasomatized lithosphere-asthenosphere interaction during slab roll-back: Evidence from Late Carboniferous gabbros in the Luotuogou area, Central Tianshan. Lithos 140-141, pp. 86–102.

Tatsumi, Y. and Suzuki, T., 2009. Tholeiitic vs Calc-alkalic Differentiation and Evolution of Arc Crust: Constraints from Melting Experiments on a Basalt from the Izu Bonin Mariana Arc. *Journal of Petrology,* volume 50 Number 8, pp. 1575-1603.

Thompson, G. M., 1998. The Geochemistry and Petrogenesis of Rarotonga, an Ocean Island in the Soutb Pacific. Upublished PhD thesis for the Memorial University of Newfoundland, 338 pp.

Verma, S. P., 2001. Geochemical evidence for a lithospheric source for magmas from Acoculco caldera, Eastern Mexican Volcanic Belt. Int Geol. Rev 43, pp. 31-51.

Wager, L. and Brown, G., 1968. Layered Igneous Rocks. Oliver and Boyd, Edinburgh, 588 pp.

Watson, E. B., 1982. Basalt contamination by continental crust: some experiments and models. Contributions to Mineralogy and Petrology 80, pp. 73-87.

Yang, Q. L., Zhao, Z. F. and Zheng, Y. F., 2012. Slab-mantle interaction in continental subduction channel: Geochemical evidence from Mesozoic gabbroic intrusives in southeastern North China. Lithos 155, pp. 442–460.

Zhao, Z. F., Dai L. Q. and Zheng, Y. F., 2013. Postcollisional mafic igneous rocks record crust-mantle interaction during continental deep subduction. Scientific Reports vol. 3: 3413, pp. 1-6.

Zi, J., Fan, W., Wang, Y., Peng, T. and Guo, F., 2008. Geochemistry and petrogenesis of the Permian mafic dykes in the Panxi region, SW China. Gondwana Research 14 (2008), pp. 368-382.